

# **JGR** Planets

### **RESEARCH ARTICLE**

10.1029/2025JE008989

#### **Key Points:**

- Deposits containing amorphous hydrated silica are present in Oxia Planum, the future landing site of the ExoMars rover
- Opal occurs stratigraphically between the clay-bearing plains and sedimentary fan, and within topographic lows to the south
- Candidate opal deposits are also present within the sedimentary fan body, and possibly in rover-accessible locations throughout Oxia Planum

#### **Supporting Information:**

Supporting Information may be found in the online version of this article.

#### Correspondence to:

J. D. McNeil, joe.mcneil@nhm.ac.uk

#### Citation:

McNeil, J. D., Grindrod, P., Tornabene, L. L., Fawdon, P., & Rangarajan, V. G. (2025). Hydrated silica in Oxia Planum, Mars. *Journal of Geophysical Research: Planets*, 130, e2025JE008989. https://doi.org/10.1029/2025JE008989

Conceptualization: Joseph D. McNeil,

Peter Grindrod, Livio L. Tornabene

Received 13 FEB 2025 Accepted 8 SEP 2025

#### **Author Contributions:**

Data curation: Joseph D. McNeil, Peter Fawdon, Vidhya Ganesh Rangarajan Formal analysis: Joseph D. McNeil, Peter Fawdon, Vidhya Ganesh Rangarajan Funding acquisition: Peter Grindrod Investigation: Joseph D. McNeil, Vidhya Ganesh Rangarajan Methodology: Joseph D. McNeil, Peter Grindrod, Livio L. Tornabene Project administration: Joseph D. McNeil, Peter Grindrod Resources: Joseph D. McNeil, Peter Grindrod, Livio L. Tornabene, Peter Fawdon, Vidhya Ganesh Rangarajan Supervision: Joseph D. McNeil, Peter Grindrod, Livio L. Tornabene

© 2025. The Author(s). This is an open access article under the terms of the Creative Commons Attribution License, which permits use, distribution and reproduction in any medium, provided the original work is properly cited.

# Hydrated Silica in Oxia Planum, Mars

Joseph D. McNeil<sup>1</sup>, Peter Grindrod<sup>1</sup>, Livio L. Tornabene<sup>2</sup>, Peter Fawdon<sup>3</sup>, and Vidhya Ganesh Rangarajan<sup>4</sup>

<sup>1</sup>Natural History Museum, London, UK, <sup>2</sup>Institute for Earth and Space Exploration, University of Western Ontario, London, ON, Canada, <sup>3</sup>School of Physical Sciences, The Open University, Milton Keynes, UK, <sup>4</sup>Institut für Planetenforschung, German Aerospace Center (DLR), Berlin, Germany

**Abstract** Hydrated silica (SiO<sub>2</sub>·nH<sub>2</sub>O; opal) is important for understanding the geological and aqueous history and habitability of Mars, owing to its genesis in a wide range of aqueous environments and its high biosignature preservation potential relative to other hydrated minerals. Utilizing multispectral CaSSIS and hyperspectral CRISM data, we investigated opal-bearing deposits in Oxia Planum, the future landing site of the ExoMars "*Rosalind Franklin*" rover, in order to further assess the region's aqueous geology and astrobiological potential. Additionally, we used CaSSIS color band ratio composites to expand the CRISM data and identify discrete deposits of hydrated silica throughout the sedimentary fan stratigraphy, and identify potential opal-bearing deposits within the *Rosalind Franklin* landing ellipses. We have detected opal-bearing material in two main physiogeographic regions of Oxia Planum: (a) stratigraphically between the clay-bearing plains and the overlying sedimentary fan, and (b) in discrete outcrops in topographic lows south of the fan deposits. Amorphous opal, likely derived from weathering processes, is the dominant form of hydrated silica in Oxia Planum. Whilst a detrital origin for the hydrated silica-bearing deposits cannot be conclusively ruled out, an authigenic origin, or one in which opaline silica is concentrated by groundwater or pedogenic silicification processes, remains the most plausible formational hypotheses. These outcrops offer exciting prospects for in situ astrobiological exploration, which will allow for these hypotheses to be tested.

**Plain Language Summary** We used orbital remote sensing data to identify deposits containing hydrated silica (opal) in Oxia Planum, the future landing site of the ExoMars *Rosalind Franklin* rover. The opal occurs between clay-rich plains and an overlying sedimentary fan, and within topographic lows south of the sedimentary fan. Compositional data indicate that opal is mostly amorphous in structure, resulting from weathering of other rocks. While we cannot rule out that some opal was transported from elsewhere, it most likely formed in place by falling out of solution or through later groundwater or soil-forming activity. We have identified opal in local regions within the fan, as well as possible opal deposits near the center of the *Rosalind Franklin* landing site, which are prime targets for the rover's search for past habitable conditions and signs of past or present life.

#### 1. Introduction

Hydrated silica (SiO<sub>2</sub>·nH<sub>2</sub>O; opal) is an important mineral in understanding aqueous processes and habitability on Mars, owing to its various formation pathways that all invariably require liquid water in its genesis and modification. Since the first detection of hydrated silica on Mars by the Miniature Thermal Emission Spectrometers (Christensen et al., 2003) onboard the Mars Exploration Rovers in Meridiani Planum (Glotch et al., 2006) and Columbia Hills (Squyres et al., 2008), opal-rich deposits have been identified across the martian surface through orbital remote sensing (e.g., Milliken et al., 2008) using visible-near-IR spectrometers such as Observatoire pour la Minéralogie, l'Eau, les Glaces et l'Activité (OMEGA; Bibring et al., 2004) and Compact Reconnaissance Imaging Spectrometer for Mars (CRISM; Murchie et al., 2007). These detections, alongside those of other aqueous minerals (e.g., phyllosilicates, sulfates, zeolites, and carbonates), reveal that extensive water-rock interactions occurred in surface and subsurface environments within past climates markedly warmer and wetter than that of present day Mars (e.g., Bibring et al., 2006; Ehlmann et al., 2011; Mustard et al., 2008; Poulet et al., 2005; Wray et al., 2008). The occurrence of hydrated silica on Mars has been attributed to three different formational mechanisms: (a) detrital, in which sediments containing silica are transported and deposited by water or wind, (b) authigenic, where silica precipitates directly from aqueous solutions within sedimentary or volcanic environments, and (c) silcretization processes, where silica is reprecipitated in concentrated layers or nodules by silicaenriched groundwater or through relative enrichment due to weathering of nearby silicate rocks (Bishop

MCNEIL ET AL. 1 of 20



# Journal of Geophysical Research: Planets

10.1029/2025JE008989

Validation: Joseph D. McNeil Visualization: Joseph D. McNeil, Livio L. Tornabene, Vidhya Ganesh Rangarajan Writing – original draft: Joseph D. McNeil Writing – review & editing: Joseph D. McNeil, Peter Grindrod, Livio L. Tornabene et al., 2008; Marzo et al., 2010; Milliken et al., 2008; Pan et al., 2021; Pineau et al., 2020; Ruff et al., 2011; Skok et al., 2010; Sun & Milliken, 2018; Voigt et al., 2024).

Two key characteristics of hydrated silica make it unique in its ability to improve our understanding of past aqueous environments and habitability on Mars. First, on Earth, as well as forming biogenically through deposition of diatom skeletons (Oehler, 1979), hydrated silica forms abiotically in a variety of aqueous environments, including as siliceous ooze in deep oceanic basins (Bohrmann et al., 1994), as cherts (sedimentary microcrystalline silica) in lacustrine basins (Eugster, 1969), as siliceous sinter in hot spring and hydrothermal settings (Boudreau & Lynne, 2012; Sun & Milliken, 2020), including those induced by meteorite impacts (e.g., Osinski et al., 2013), and in volcano-fumarolic settings (Seelos et al., 2010). These diverse formation settings demonstrate that hydrated silica is not uniquely diagnostic of any one process but rather a product of diverse processes in a range of aqueous environments. Second, in terrestrial environments, hydrated silica acts as an extremely effective preservation agent for physical and chemical biosignatures relative to other minerals (McMahon et al., 2017; Orange et al., 2009, 2013). Some of the oldest unambiguous terrestrial biosignatures are observed in silicified phases (e.g., Schopf, 1993), and exceptional preservation of plant/animal matter within an opal framework has been documented (Chauviré et al., 2020; Rondeau et al., 2012). Silicic acid, formed through the interaction of silica and water, readily bonds to cell walls and envelopes, with this process occurring across a large range of temperatures, salinities, and pH levels, agnostic of cell type (Butts, 2014). Consequently, permineralized biological material including cells, organic carbon, molecular fossils such as lipids, and microbialites (e.g., stromatolites) are exceptionally well-preserved within rocks with high silica content (e.g., Duda et al., 2016; Gouzy et al., 2025). Well-preserved organic biomarkers are present in such deposits even after lithification, diagenesis, and exposure to subsequent subsurface aqueous conditions (e.g., Rhynie Chert, Scotland; Garwood et al., 2020), owing to the innate impermeability and resistance to chemical weathering that is characteristic of hydrated silica. As such, deposits with high silica content on Mars are excellent candidates for retaining details of past aqueous environments, and if those environments were habitable, any biosignatures that were present.

Oxia Planum is the future landing site of the ESA ExoMars "Rosalind Franklin" rover (RFR; Figure 1), which will search for physical and chemical biosignatures at the surface and subsurface using its analytical suite of instruments, the "Pasteur" payload (Vago et al., 2017). Located on the margin of the rugged, Noachian-aged highlands of Arabia Terra and the smooth, low-lying, Hesperian-aged plains of Chryse Planitia, the Oxia Planum region contains an exceptional geomorphological and geochemical record of ancient Noachian surface and subsurface environments, with abundant evidence of past aqueous activity (Fawdon et al., 2022; Quantin-Nataf et al., 2021). This evidence includes fractured, layered, phyllosilicate-bearing plains, which are indicative of widespread water-rock interactions and are the primary astrobiological target of the rover (Brossier et al., 2022; Davis et al., 2023; Mandon et al., 2021; Parkes-Bowen et al., 2022; Quantin-Nataf et al., 2021), a sedimentary fan, associated with Coogoon Vallis that could indicate a standing body of water in the Oxia basin as part of a regional hydrological system (Quantin-Nataf et al., 2021; Roberts et al., 2024), and widespread depositional, erosional, and impact-related processes that shaped the ancient landscape (Favaro et al., 2021; McNeil et al., 2022; Quantin-Nataf et al., 2021; Roberts et al., 2021). Deposits rich in hydrated silica have been detected in the south of the landing site associated with the sedimentary fan (Figure 1; Carter et al., 2023; Pan et al., 2021; Quantin-Nataf et al., 2021), but little work has been done to expand on this observation. As such, the true stratigraphic position of hydrated silica-bearing material, as well as its geographic range, and crucially, its geochemistry and possible origins, are not currently understood.

Here we present the first comprehensive study that focuses on the silica-rich deposits in Oxia Planum, aimed at unraveling their origins, stratigraphic relationships with other key landing site units, and relevance to RFR mission objectives. Utilizing available hyperspectral CRISM cubes, we investigated the mineralogy of hydrated silica-bearing deposits around the south of the landing site near the sedimentary fan and Noachian highland units. Additionally, we have augmented these detections with multispectral Color and Stereo Surface Imaging System (CaSSIS; Thomas et al., 2017) and High Resolution Imaging Science Experiment (HiRISE; McEwen et al., 2007) data, employing color band ratio composites (CBRCs; Tornabene et al., 2018), which not only constrain our CRISM detections of hydrated silica to specific morphostratigraphic units at higher spatial resolutions but also expand the detection beyond the spatial limitations of hyperspectral CRISM data alone.

MCNEIL ET AL. 2 of 20

21699100, 2025, 9, Downloaded from https://aggubts.onlinelibrary.wiley.com/doi/10.109/2025IE008989 by Disch Zentrum F. Luft-U. Raum Fahrt in D. Helmholtz Gemein.

Wiley Online Library on [01/10/2025]. See the Terms and Condition

Figure 1. Regional geography of Oxia Planum. (a) CTX DTM showing elevation and 3-sigma 2028 landing ellipses for the ExoMars RFR mission (orange: launch opportunity 1 (LO1), yellow: launch opportunity 2 (LO2)). Inset Mars Orbiter Laser Altimeter globe indicates Oxia Planum's location near the dichotomy boundary between Arabia Terra (AT) and Chryse Planitia (CP). The sedimentary fan is outlined in black dots, and the northern and southern Neocoogoon Valles (NCV) are indicated by blue dotted lines. Mars Orbital Catalog of Aqueous Alteration Signature (MOCAAS) locations of silicate minerals (Carter et al., 2023) shown in cyan correspond to 100 m/pixel detections of hydrous aluminosilicates or hydrated silica (locally in Oxia Planum refined to "hydrated silica  $\pm$  kaolins"). (b) CaSSIS NIR-PAN-BLU (NPB) mosaic of the fan region, with the margins of the fan outlined. MOCAAS hydrous aluminosilicates/hydrated silica shown as cyan outlines. (c) CaSSIS NPB mosaic of Pelso Chasma, south of the fan. The quasi-circular shape of Pelso Chasma is indicated by a dotted line. Geographic nomenclature follows the scheme of Fawdon et al. (2021).

# 2. Methods

All available CaSSIS data in the southern Oxia Planum landing site region were acquired from the University of Bern's CaSSIS data repository and incorporated into a geographic information system (GIS) in ArcGIS Pro 3.2.2. CaSSIS data were georeferenced to a basemap mosaic of HiRISE RED mosaic images (Tao et al., 2021) of the region, which also has a corresponding Context Camera (CTX; Malin et al., 2007) mosaic and CTX Digital Terrain Model (DTM; Tao et al., 2021) from which elevations were derived. Additional HiRISE images were acquired from the Planetary Data System (PDS) on an individual basis and added to the GIS.

# 2.1. Hyperspectral CRISM Data

Hydrated silica possesses characteristic near-infrared absorption features centered around 1.4  $\mu$ m (stretching overtones of Si-OH at ~1.41  $\mu$ m and H<sub>2</sub>O-OH at ~1.46  $\mu$ m), near 1.9  $\mu$ m (H<sub>2</sub>O combination bending and stretching modes at 1.91 and 1.96  $\mu$ m) and 2.2  $\mu$ m (a combination of OH stretching and Si-OH bending modes at ~2.21  $\mu$ m), from free silanols (Si-OH) and ~2.26  $\mu$ m, from hydrogen-bonded silanols (Brown et al., 2003; Burneau et al., 1990; Langer & Flörke, 1974; Rice et al., 2013). Whilst the 1.4 and 1.9  $\mu$ m absorptions are common amongst hydrated minerals, the 2.2  $\mu$ m feature is exclusive to hydrated silica and Al-bearing phyllosilicates. Hydrated silica and Al-phyllosilicates can be distinguished based on the broadness of the 2.2  $\mu$ m absorption, which is narrower in Al-bearing phyllosilicates owing to the lack of a 2.26  $\mu$ m contribution from hydrogen-bonded silanols (Ehlmann et al., 2009; Langer & Flörke, 1974; Milliken et al., 2008; Rice et al., 2013).

Oxia Planum was selected as a landing site in 2018, long after CRISM faced issues such as aging detectors, cryocoolers, and gimbals (utilized for targeted observations), following its nominal mission phase (Seelos et al., 2024). As such, very few good quality full-resolution targeted CRISM data sets exist in the landing site

MCNEIL ET AL. 3 of 20

region, with most hyperspectral data limited to noisy and/or lower spatial and spectral resolution CRISM data. Previous work identified hydrated silica in the south of the landing site associated with the sediment fan (Carter et al., 2023; Pan et al., 2021; Quantin-Nataf et al., 2021), and as such, our search primarily focussed on this region. We analyzed all available targeted CRISM data in the southern Oxia Planum region (Figure S1 in Supporting Information S1) and rejected those without hydrated silica detections. Of the cubes with positive hydrated silica detections, we identified one Full-Resolution Targeted (FRT) data cube that possessed appropriately high signal-to-noise ratios: 9A16, and three Along-Track Undersampled (ATU) data cubes (3D04C, 38B10, 3561F). ATU3561F was not included owing to its shared footprint with FRT9A16, which has a much better signal-to-noise ratio and higher spatial resolution.

CRISM I/F (where I is the radiance on the sensor, and F is the expected solar radiance during the observation, if the atmosphere had been removed) FRT and ATU cubes were acquired from the NASA PDS in TRDR (and MTRDR where available) formats. Subsequent processing and analyses of the data followed standardized techniques (Ehlmann et al., 2009; Milliken et al., 2010), with photometric corrections applied to correct for viewing geometry, and atmospheric corrections made using the volcano scan method (McGuire et al., 2009), allowing for removal of contributions from atmospheric CO<sub>2</sub>. These processing steps were conducted in the CRISM Analysis Toolkit 7.4 (CAT; Morgan et al., 2017), a software package developed by the CRISM team as an extension to the Environment for Visualizing Images (ENVI) 8.8.1 image processing and analysis software.

An additional empirical "dark subtraction (DS)" processing step was undertaken after the initial processing to address scatter from time-variable atmospheric aerosol contributions not addressed by the volcano scan method and maximize our ability to identify hydrated silica-bearing regions. DS, a common terrestrial remote sensing technique (e.g., Armstrong, 1993; Chavez, 1988; Wicaksono & Hafizt, 2018), assumes that the darkest pixels in an image contain very little contribution from the surface, and that these pixels represent contributions from atmospheric scattering, which on Mars is dominated by ferric iron oxide "dust" (e.g., Tornabene et al., 2018). This "dark" component, often but not always represented by the absolute minimum values in the scene, was assessed based on location (originating from a dark shadow or dark spectrally low contrast surface) and subtracted from all other pixels in the cube, which thereby reduces the scattering contribution and results in spectral shapes more consistent with the surface components (Rangarajan et al., 2024; Tornabene et al., 2021, 2022). When a DS correction is successfully applied to CRISM data, it may serve as a useful and beneficial alternative to the traditional "ratioing method" that involves ratioing a spectrum with that from a spectrally bland region in the same detector column, which is often challenging to confidently locate for many cubes. For our study, it means that individual pixels—perhaps representing the visible extent of a small outcrop of hydrated silica—can be interrogated without ratioing to another pixel, and thus, these DS-corrected cubes were used exclusively as a guide for where to find the strongest hydrated silica signals. DS was undertaken multiple times using several different, manually selected "dark" pixels (i.e., from the shadowed walls of craters or topographic prominences) from across the cube, in order to ensure that the resultant DS-corrected cube was not altered significantly by errant noise in the selected "dark" pixels.

DS cubes were surveyed using a combination of summary parameters from Viviano-Beck et al. (2014) that highlight hydrated silica and allow for differentiation between Si- and Al-hydroxylated minerals. Specifically, the MIN2250 (2.21  $\mu$ m Si-OH band depth and 2.26  $\mu$ m H-bound Si-OH band depth), BD2250 (band depth at Al-OH 2.25  $\mu$ m absorption), and BD1900R2 (band depth at 1.9  $\mu$ m indicative of bound H<sub>2</sub>O) parameters were used to highlight candidate hydrated silica-bearing regions of interest. Candidate regions of interest were then manually inspected within the DS cubes to confirm the presence of characteristic hydrated silica spectral features. Once verified, the spatial locations of these ROIs were transferred to the corresponding pixels in the original non-DS I/F-corrected cubes. Spectra from these cubes were then ratioed to a corresponding spectrally bland "denominator" region (Ehlmann et al., 2009; Milliken et al., 2010) in the same detector column in order to remove systematic instrument artifacts and atmospheric residual artifacts and to emphasize the compositional differences between the area of spectral interest and the reference region (Bishop et al., 2008; Ehlmann et al., 2009; Milliken et al., 2010).

Next, near-infrared spectra from these regions were processed following a similar method as in Pineau et al. (2020). Spectra were first smoothed using a Savitsky-Golay filter using a third-degree polynomial function and an eight-point moving average window (Savitzky & Golay, 1964; Steinier et al., 1972), wherein resultant "smoothed" spectra retained the positions of local minima and maintained a high signal-to-noise ratio. Next, the

MCNEIL ET AL. 4 of 20

smoothed spectra underwent continuum removal in ENVI 8.8.1 using a segmented upper hull method (Clark et al., 1987). The position of the band minima for the key 1.4, 1.9 and 2.2  $\mu$ m absorptions were measured manually from the resultant spectra. The error associated with these manual measurements was estimated to be no more than  $\pm 0.005~\mu$ m through repeated measurement attempts. In order to analyze the shape of each absorption feature, the individual features were isolated from the rest of the spectrum at anchor points positioned at 1.32 and 1.60  $\mu$ m, 1.82 and 2.13  $\mu$ m, and 2.13 and 2.37  $\mu$ m (after Pineau et al., 2020). These clipped spectra were then subjected to Gaussian deconvolution in Origin Pro 8.5 software, with each Gaussian function placed according to the spectral absorptions outlined in Pineau et al. (2020). From these deconvolved, clipped spectra, we calculated the concavity ratio criterion (CRC), which has been used to identify hydrothermal versus weathering-derived opal (Chauviré et al., 2017), and for the 2.2  $\mu$ m feature, the ratio of the band depths at 2.26 and 2.21  $\mu$ m was also calculated (henceforth referred to as 2.2R), a well-established proxy for the crystallinity of martian opal (e.g., Sun & Milliken, 2018). The error associated with the CRC measurements is given as 2 × Standard Error of the Mean. Errors associated with band depth ratios (assuming each band depth measurement was no more than  $\pm 5\%$  from the true value) were calculated using standard ratio error propagation and therefore differed between data points.

#### 2.2. CaSSIS Color Band Ratio Composites

Four-band CaSSIS data that covered the southern portion of the landing site were subjected to a pipeline that included DS and band ratio calculations to produce CBRCs that include parameters to assess the quality of the DS correction, and to aid in mineralogic analysis across a much wider area and higher spatial resolution than the CRISM data allows (Tornabene et al., 2018). Alongside the four CaSSIS bands (NIR (band center 939 nm), RED (band center 836 nm), PAN (band center 675 nm), BLU (band center 495 nm)), parameters were calculated from them that include ratios which positively discriminate between ferric and ferrous material, as well as water ice, bound water, and chlorides (for a description of these combinations, see Rangarajan et al., 2023, 2024; Tornabene et al., 2018). Due to different viewing geometries, atmospheric effects, and lighting conditions, individual combinations of CBRCs were permutated manually on an image-by-image basis in regions of confirmed CRISM hydrated silica detections in order to determine the best combinations to highlight silica-rich material from other deposits. We found that CBRC combinations of BLU-RPR-PBR in R-G-B uniquely highlighted these outcrops in a reddish-pink hue in most images and allowed us to expand our detections to nearby morphologically similar outcrops that do not have hyperspectral coverage or are below the spatial resolution of CRISM. This combination highlights silica-rich materials based on its relative lack of dust or ferric or ferrous iron relative to the bulk of Mars, its overall brightness and relatively flattened spectrum when compared with other common materials on Mars. This has allowed us to identify additional hydrated silica-bearing deposits, as well as prospective outcrops that are closer to the center of the RFR landing ellipses that could be realistic astrobiologically relevant targets for the rover to sample.

#### 2.3. HiRISE Color Band Ratio Composites

Similarities between the spectral responses of the three HiRISE and four CaSSIS bands (McEwen et al., 2007; Thomas et al., 2017) allow for a similar product to CaSSIS CBRC BLU-RPR-PBR to be created for HiRISE, with the equivalent combination BG-(IR/RED)-(RED/BG) theoretically able to highlight hydrated silica-bearing materials in a similar way. The main benefits of this are two-fold: first, as a confirmatory step of the CaSSIS CBRC methodology using a second instrument, and second, to identify possible hydrated silica-bearing deposits at a much higher resolution (~50 cm/pixel) than is available with CaSSIS. Unfiltered HiRISE data products, that is, those which have not undergone cosmetic clipping of values at both ends of the image histogram (e.g., Daubar et al., 2016; Rangarajan et al., 2024), were generated by running a series in ISIS (Sucharski et al., 2020) of algorithms developed based on the internal processing pipelines used by the HiRISE team. Similar to the CaSSIS processing steps, a DS correction was also applied to the HiRISE color products to help mitigate the effects of time-variable atmospheric scatter. Finally, color band ratio composites in the combination BG-(IR/RED)-(RED/BG) generated from the resultant unfiltered HiRISE were used to gain additional detail and information on outcrops already identified using CaSSIS CBRCs.

MCNEIL ET AL. 5 of 20

# 3. Results

# 3.1. Geographic Distribution of Hydrated Silica in Oxia Planum

We have identified deposits of hydrated silica in two broad geographic locations in the southern Oxia Planum region. These are: (a) directly adjacent to sedimentary fan material (Figure 2), and (b) within large topographic lows, such as the Pelso Chasma region and valleys directly south and southeast of the fan (Figure 3). Whilst the detections are not individually spatially extensive, they occur over a broad geographic range across an area of  $\sim$ 85 km<sup>2</sup>.

Near the fan (Figure 2a), CRISM detections correlate with either bright-toned, bluish-white bedrock that appears fractured at the decameter scale in CaSSIS NPB and HiRISE IR-RED-BG (IRB) data, or with darker surfaces directly adjacent to outcrops of the same material, suggesting that opaline material is present in the bright bedrock layer, and is undergoing contemporaneous erosion into unconsolidated material in the surrounding regions. Where it is exposed, this hydrated silica-bearing unit (HSU) is <5 m in thickness and occurs stratigraphically above the phyllosilicate-bearing plains materials and below the sedimentary fan (Figures 2b and 2c). Similar, extremely thin (<2 m) bright-toned outcrops are visible in discontinuous horizons within exposed crater walls within the sedimentary fan material at the HiRISE scale (Figure 2d), and as discontinuous strata on exposed faces of the fan (Figure 2e). In the HSU, bright concentric material, morphologically similar to other features observed within degraded impact craters across the landing site, occurs stratigraphically directly below outliers of fan sediments (Figure 2f). Other features that are morphologically similar to these bright concentric deposits occur directly on top, and interbedded within, the fan material across its spatial and stratigraphic extent (Figures 2g–2i). The elevation range of these fan-adjacent detections across the region is approximately 35 m over a horizontal distance of 9 km.

The second geographic context in which hydrated silica has been detected is within the topographic lows located south of the sedimentary fan (Figure 3a). The HSU here, much like in the fan, is also bright-toned (Figure 3b), but the fracturing is closer to meter-scale than decameter scale (Figure 3c). The valley walls that these outcrops adjoin are made of Fe/Mg-phyllosilicate-bearing unit material, owing to the elevation of these horizontally layered units to the northwest, and because we observe possible Fe/Mg-phyllosilicate-bearing outcrops cropping out of the valley walls (Figure S2 in Supporting Information S1). Phyllosilicates have been detected up to 250 m below the surface of the plains (Quantin-Nataf et al., 2021), suggesting that the valley walls, which reach a depth of ~100 m below the plains, likely consist of the same material. We observe no evidence that the HSU unit here forms part of the cliff. HSU also crops out on the central valley floor, and occurs as slightly raised topography (Figure 3d), suggesting that HSU was deposited here post-valley incision. We also observe possible HSU outcrops further east in the floor of North Neocoogoon Vallis (Figure S3 in Supporting Information S1). Within the valley region, HSU is mostly obscured by TARs (Transverse Aeolian Ridges), and a thin veneer of younger bedrock that is dark, spectrally bland, and similar in nature to the dark infilling material (DIM) that manifests throughout Oxia Planum as upstanding mesas, inverted channels, and crater fill (Harris et al., 2024).

# 3.2. Tandem Multi- and Hyperspectral Observations of Hydrated Silica

CBRCs enable detection of candidate HSU outcrops beyond the spatial coverage or resolution of targeted CRISM data (Figure 4) by highlighting CRISM-confirmed HSU in a distinctive color, allowing contiguous or adjacent outcrops with similar morphology, elevation, geographic position, and stratigraphic context to be recognized as likely belonging to the same unit. In addition to the CRISM-confirmed HSU, the CBRCs highlight other areas around the base of the sedimentary fan (Figures 4b and 4c), as well as discontinuous bright-toned outcrops within the fan's internal stratigraphic architecture that have been exposed by impacts that have occurred through the fantop (Figure 4d), and outcrops directly on the top of the sedimentary fan (Figure 4e). These bright strata show that this unit, likely a continuation of HSU, is not continuous under the fan, and either formed in discrete locations and/or was heavily eroded before emplacement of the sedimentary fan. This would explain why outcrops of hydrated silica are not ubiquitously detected at the fan-plains contact. Additionally, they show that HSU occurs multiple times within the fan stratigraphy.

In addition, they also highlight two other groups of features in Oxia Planum (Figure 5), which have distinct physiogeographic and stratigraphic characteristics, and could therefore have similar opal-bearing compositions: bright crater fill (BCF) and bright rocky outcrops (BRO). BCFs are features occurring as relatively bright, light-

MCNEIL ET AL. 6 of 20

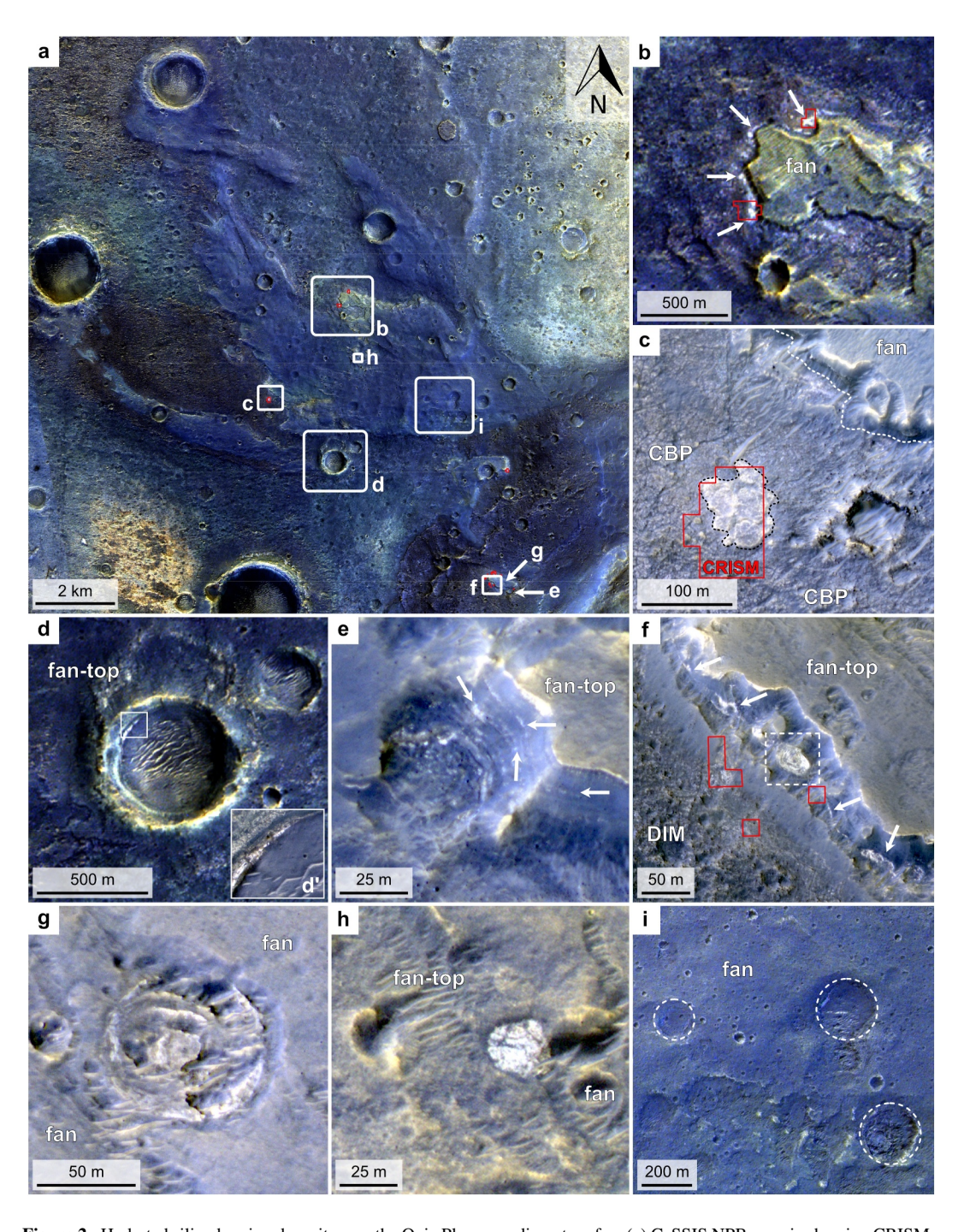


**Figure 2.** Hydrated silica-bearing deposits near the Oxia Planum sedimentary fan. (a) CaSSIS NPB mosaic showing CRISM detections (red) and locations of panels (b–i) (white). List of component images included in supplementary materials. (b) CaSSIS NPB shows white material at the fan's edge corresponding to CRISM silica detections. (c) HiRISE IRB ESP\_043268\_1980 shows bright-toned, isolated, fractured silica-bearing material at base of fan above clay-bearing plains (CBP). (d) CaSSIS NPB showing a 500 m-diameter crater revealing fan stratigraphy, including a discontinuous bright white layer likely composed of hydrated silica. (e) HiRISE IRB ESP\_037703\_1980 shows white-toned, possibly opal-bearing horizons in an outcrop of fan material. (f) HiRISE IRB ESP\_037703\_1980 showing thin white material at the fan's base, aligning with CRISM silica detections including concentric crater-fill (white box). (g) HiRISE IRB ESP\_037703\_1980 of an eroded concentric deposit interpreted as a crater infilled with sedimentary material. (h) HiRISE IRB ESP\_060437\_1980 of bright fractured material near the fan's top, resembling opal-bearing deposits. (i) CaSSIS-HiRISE pansharpened image of buried craters near the fan's top.

MCNEIL ET AL. 7 of 20

**Figure 3.** Hydrated silica deposits south of the sedimentary fan. (a) CaSSIS NPB mosaic of Pelso Chasma with CRISM silica detections (red) and panel locations (b–d) (white). (b) CaSSIS NPB showing a CRISM silica detection (red) at the valley's western edge, corresponding to an extensive, bright outcrop that is partially obscured by dark infilling material (DIM). (c) HiRISE IRB ESP\_077041\_1980 showing the locations of CRISM detections near the northern rim of the western valley, likely a continuation of the deposit in panel (b). (d) HiRISE IRB ESP\_037703\_1980 showing bright material on the northern valley floor, covered by later deposits and transverse aeolian ridges.

toned, often bluish material within topographic lows such as highly degraded impact craters (Figure 5). As such, they are usually circular, and their upper surfaces are either fractured or concentric in texture. BCF occur in impact craters within the clay-bearing plains, that is, at the same stratigraphic horizon as the HSU (Figures 5b-5d), as well as in the upper surface of the fan itself (Figures 2f-2i and 4e). Seventy-eight outcrops of BCF were detected across the Oxia Planum region (Figure 5), identified through their stratigraphic position (above the ancient clay-bearing plains and below younger DIM), their morphology (non-extensive and texturally concentric or with a fractured upper surface similar to confirmed HSU deposits), and multispectral properties (i.e., bluer than the surrounding material, and appearing in pink hues distinct from the surrounding plains in CaSSIS CRBC BLU-RPR-PBR combination). We have identified 22 outcrops of BCF within the 2028 RFR 3-sigma landing ellipses (across both the early and late launch opportunities), making them prime candidates for in situ astrobiological investigation by RFR. Geochemical analysis of the BCFs, which share similar texture (HiRISE), color (CaSSIS), and stratigraphic position with confirmed HSU deposits, is crucial as they may provide the only realistic opportunity for RFR to investigate opal-bearing material, given the distance from the landing site center to confirmed HSU detections. The lack of high-quality hyperspectral data over BCF, the diameters of which rarely exceed the 18 m minimum spatial resolution of CRISM, means that other mineral phases which are bluer than the surrounding units, and which are predominantly ferrous, cannot be ruled out; the example in Figures 5b-5d, for example, has also been highlighted as a candidate chloride-bearing deposit (Bickel et al., 2024). Other bright rocky outcrops (BRO) are observed on irregularly shaped low-relief prominences within the clay-bearing plains (Figure 4), but we were unable to extract a spectrum with clear absorption features. BRO are similar in NPB and CBRC color to HSU outcrops, except with increased brightness and blueness. These outcrops can be seen to crop out as distinct discontinuous horizons in the walls of Pelso Chasma and on the surrounding highlands. Given these differences in color, stratigraphic position, and spectral properties, it seems likely that the BRO is unrelated to the HSU.

MCNEIL ET AL. 8 of 20

, 2025, 9, Downloaded from https://agupubs.onlinelibrary.wiely.com/doi/10.1029/2025E008989 by Dsch Zentrum F. Luft-U. Raum Fahrt n.D. Helmholtz Gwein, Wiley Online Library on (01/10/2025]. See the Terms and Conditions (https://onlinelibrary.wiely.com/term

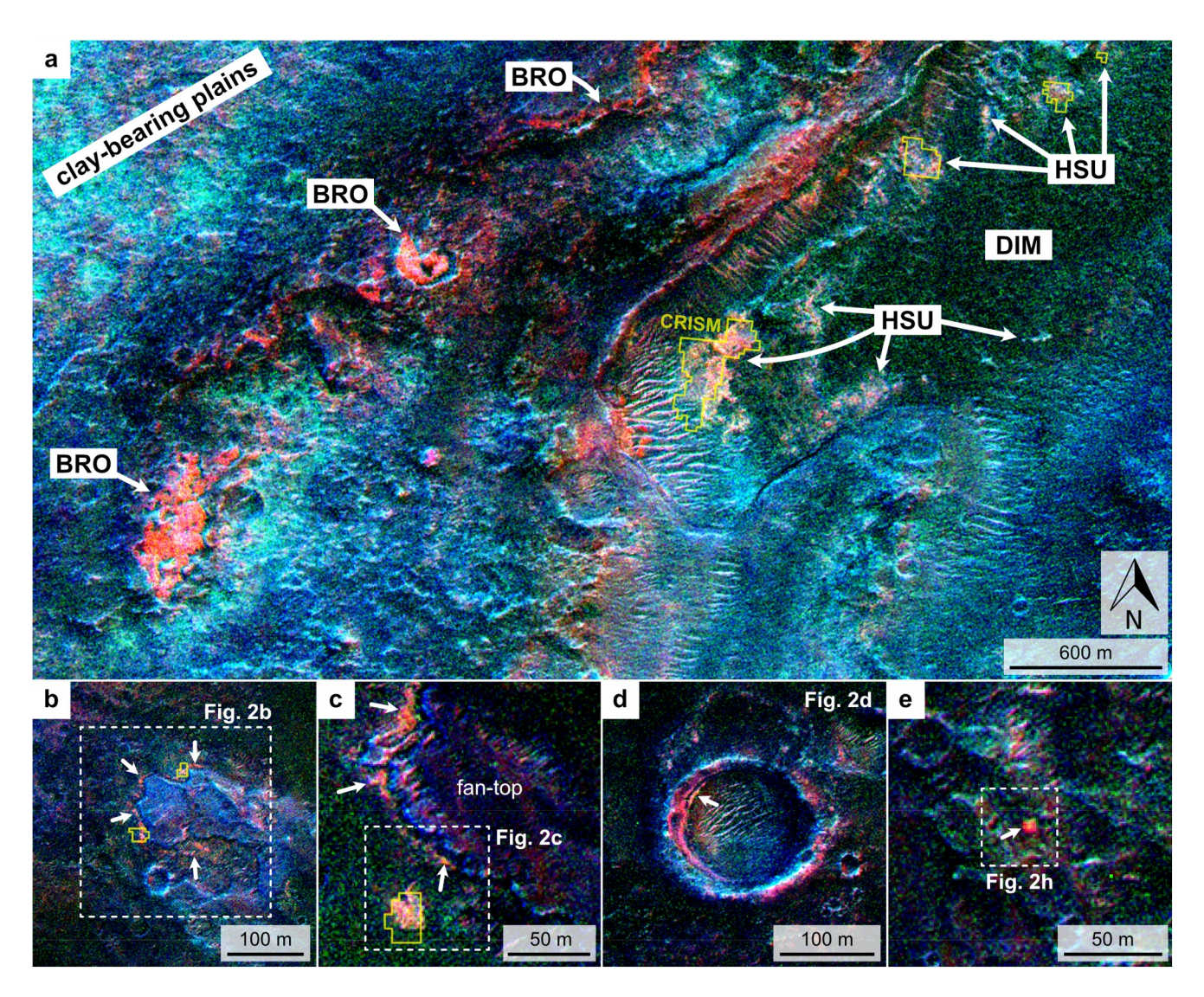
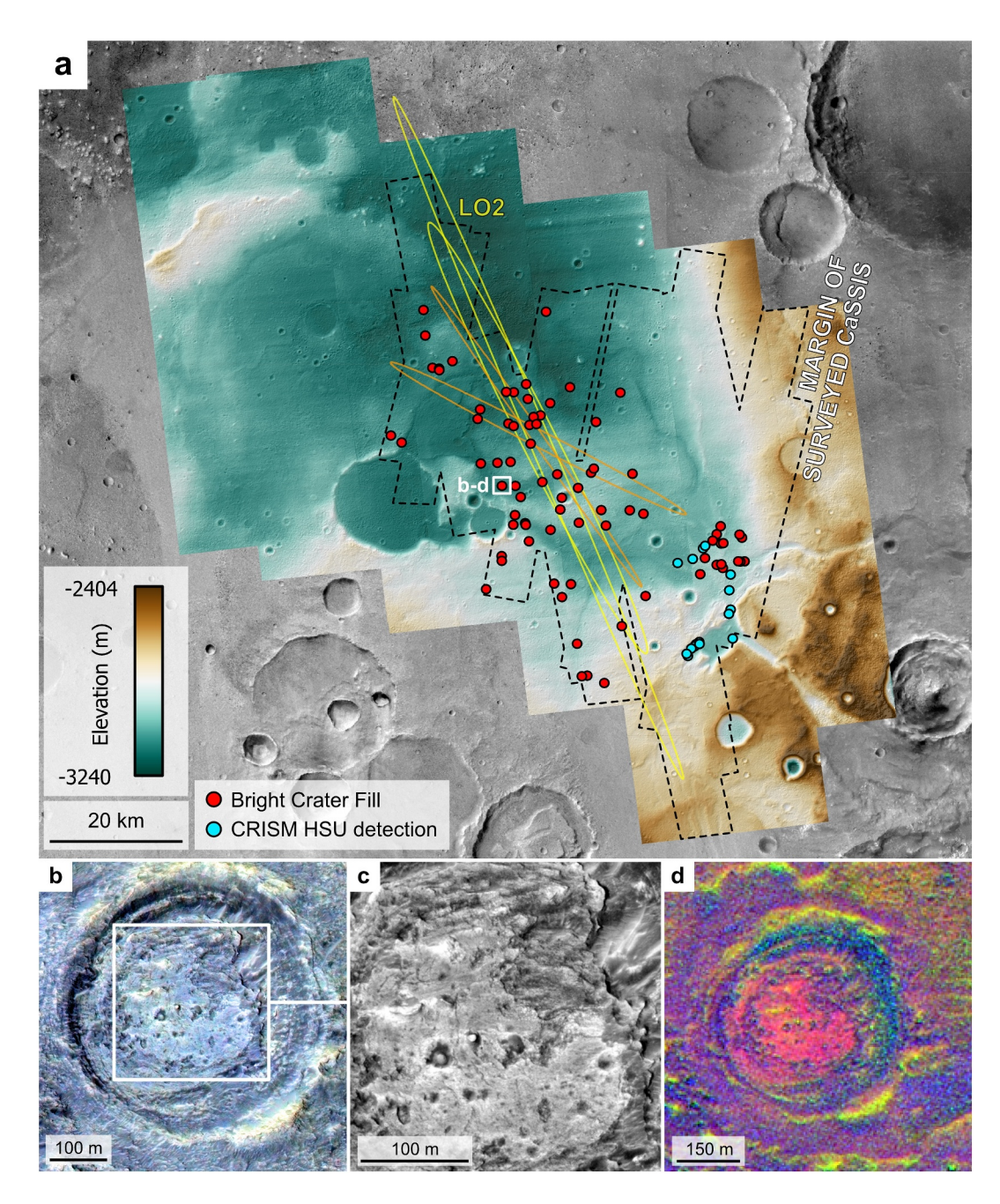


Figure 4. CaSSIS color band ratio composite (CBRC) BLU-RPR-PBR, highlighting opal-bearing materials in Pelso Chasma and the Oxia Planum sedimentary fan. (a) Western Pelso Chasma (MY37\_023007\_019): salmon-pink areas correspond to CRISM hydrated silica unit (HSU) detections (yellow); brighter red regions indicate bright rocky outcrops (BRO). Some HSU regions, not detected by CRISM due to limited exposure or dust coverage, are visible here due to the higher spatial resolution of CaSSIS. Bedrock is shown in blue-green, indicating mixed ferrous and ferric mineralogy, or in darker shades representing the spectrally bland DIM. (b) Fan-toe area (MY37\_023007\_019) with HSU below the edge of the fan, corresponding to Figure 2b. (c) Fan edge (MY37\_023007\_019) showing the outcrop from Figure 2c and similarly colored material around the fan as in panel (b). (d) Discontinuous salmon-pink outcrop in a crater wall (MY36\_021955\_163), corresponding to Figure 2d, suggesting that other HSU outcrops may be buried within the fan. (e) Exposed impact crater on the fan top, as seen in Figure 2h. In all panels the CBRCs have been manually stretched to highlight the differences between the HSU and other materials.

# 3.3. Structure and Origin of Hydrated Silica in Oxia Planum

We have obtained 14 spectra (Figure 6), which exhibit absorption features around 1.4, 1.9, and 2.2  $\mu$ m, and vary in distinctness and strength of absorption features, but are collectively characteristic of hydrated silica (Kokaly et al., 2017; Langer & Flörke, 1974). Of these spectra, 11 possess 1.4  $\mu$ m band centers at shorter wavelengths and marginally elevated 2.2R values indicative of amorphous hydrated silica (opal-A; Figure 7a). Two spectra have 1.4  $\mu$ m band centers at higher wavelengths and slightly lower 2.2R values, and plot within the crystalline (opal-CT) field. One spectrum falls in the overlap region between these fields and therefore cannot be attributed to either. There is substantial variation in the position of the 1.4  $\mu$ m band center across all detections; this does not appear to be affected by the specific cube from which a given spectrum was obtained, or the geographic location or geological context of the detection (Figure 7a). Spectrum 3D04C shows an additional asymmetrical absorption around  $\sim$ 1.75  $\mu$ m, possibly indicative of intermixing of sulfate phases with hydrated silica. Spectra 38B10-2 and

MCNEIL ET AL. 9 of 20



**Figure 5.** Locations of 78 potential hydrated silica-bearing outcrops (bright crater fill; BCF) in Oxia Planum found using CaSSIS/HiRISE CBRCs. (a) CTX DTM showing BCF locations (red dots) near the 3-sigma landing ellipses for 2028 launch opportunities one (LO1) and two (LO2). Hydrated silica-bearing unit detections using CRISM are shown in light blue. The extent of CaSSIS data surveyed for these features is shown with a black dotted line. (b) HiRISE RED (ESP\_046156\_1980) with CaSSIS NPB (MY35\_008275\_165) overlay showing bright blue BCF material filling a crater west of the landing ellipses. (c) HiRISE RED (ESP\_046156\_1980) showing BCF surface texture. (d) CaSSIS CBRC (BLU-NPR-PBR, MY35\_008275\_165) of BCF within the crater.

38B10-3 also possess a doublet feature at 2.2 and 2.3  $\mu m$  that could represent a mixture of two or more phyllosilicate phases, namely Fe/Mg-phyllosilicates and Al-phyllosilicates, or Fe/Mg-phyllosilicates with hydrated silica, or, as observed in the Mawrth Vallis region, phyllosilicate-sulfate assemblages associated with evaporitic environments (Bishop et al., 2020). No other HSU spectra contain these features, and given that the outcrops these relate to are continuous with unambiguously hydrated silica-bearing outcrops, it is likely these are localized phenomena.

MCNEIL ET AL. 10 of 20

Wiley Online Library on [01/10/2025].

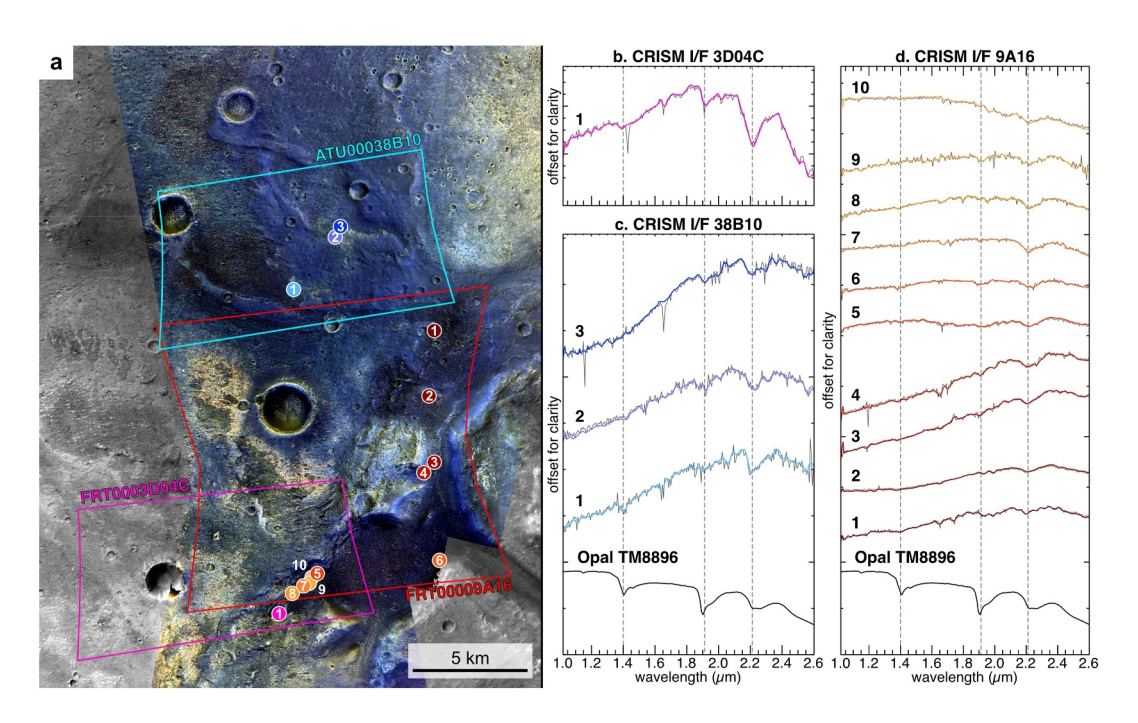


**Figure 6.** Hydrated silica detections from CRISM cubes FRT0003D04C, ATU00038B10, and FRT00009A16. (a) CTX and CaSSIS NPB mosaic showing cube locations and corresponding spectra. (b) I/F spectrum from FRT0003D04C. (c) I/F spectra for ATU00038B10 and USGS spectral reference TM8896. (d) I/F spectra for FRT00009A16 and USGS spectral reference TM8896. Characteristic 1.4, 1.9, and 2.2 μm absorptions indicated by vertical dashed lines. Both the Savitsky-Golay smoothed (colored) and non-smoothed (gray) spectra are shown.

CRC values for the 1.9 and 1.4  $\mu$ m absorption features heavily favor a weathering origin (Figure 7). 7 of the 11 resolvable CRC plots in the weathering field for the 1.9CRC, 3 CRC in the transitional zone between weathering and hydrothermal, and 1 CRC in the hydrothermal field. 10 of 12 resolvable CRC plots in the weathering field for the 1.4CRC, with the remaining 2 plotting in the hydrothermal field. The consistently low position of the 1.4  $\mu$ m absorption, along with overall low 1.4 and 1.9CRC values (Figures 7b and 7c), suggest the presence of relatively pristine dehydrated amorphous opal. This observation is in contrast with the characteristics of opal-bearing aeolian deposits (Pineau et al., 2020; Sun & Milliken, 2018) and is indicative of low-temperature weathering processes consistent with both authigenic and detrital origins.

#### 4. Discussion

# 4.1. Stratigraphic Position of Opal in Oxia Planum

The lack of elevation variability and overall similar elevation ranges of outcrops in both sedimentary fan and Pelso Chasma/Valley settings (Figure S5 in Supporting Information S1) suggests that at the time, or across the period, of HSU emplacement, the palaeotopography of the Oxia region was broadly similar as it is today, that is, much of the proposed regional erosion of the upper sections of the clay-bearing plains (e.g., McNeil et al., 2022; Quantin-Nataf et al., 2021; Roberts et al., 2021) had already taken place. By association, the occurrence of hydrated silica-bearing material within Pelso Chasma and the surrounding valleys requires those topographic depressions to have been formed by this time as well. The presence of HSU stratigraphically below and within the body of the sedimentary fan indicates that conditions for hydrated silica emplacement occurred multiple times (i.e., both before and during fan sedimentation) or that the hydrated silica was emplaced through silcretization processes post-depositionally (see Section 4.3 for discussion). The generally discontinuous nature of these outcrops implies that the formation of hydrated silica-bearing deposits was likely confined to localized areas with favorable environmental conditions, or topographic depressions that acted as sedimentary sinks, concentrating silica deposits.

MCNEIL ET AL. 11 of 20

aded from https://agupubs.onlinelibrary.wiley.com/doi/10.1029/2025JE008989 by Disch Zentrum F. Luft-U. Raum Fahrt In D. Helmholtz Gemein.,

Wiley Online Library on [01/10/2025]. See the Terms

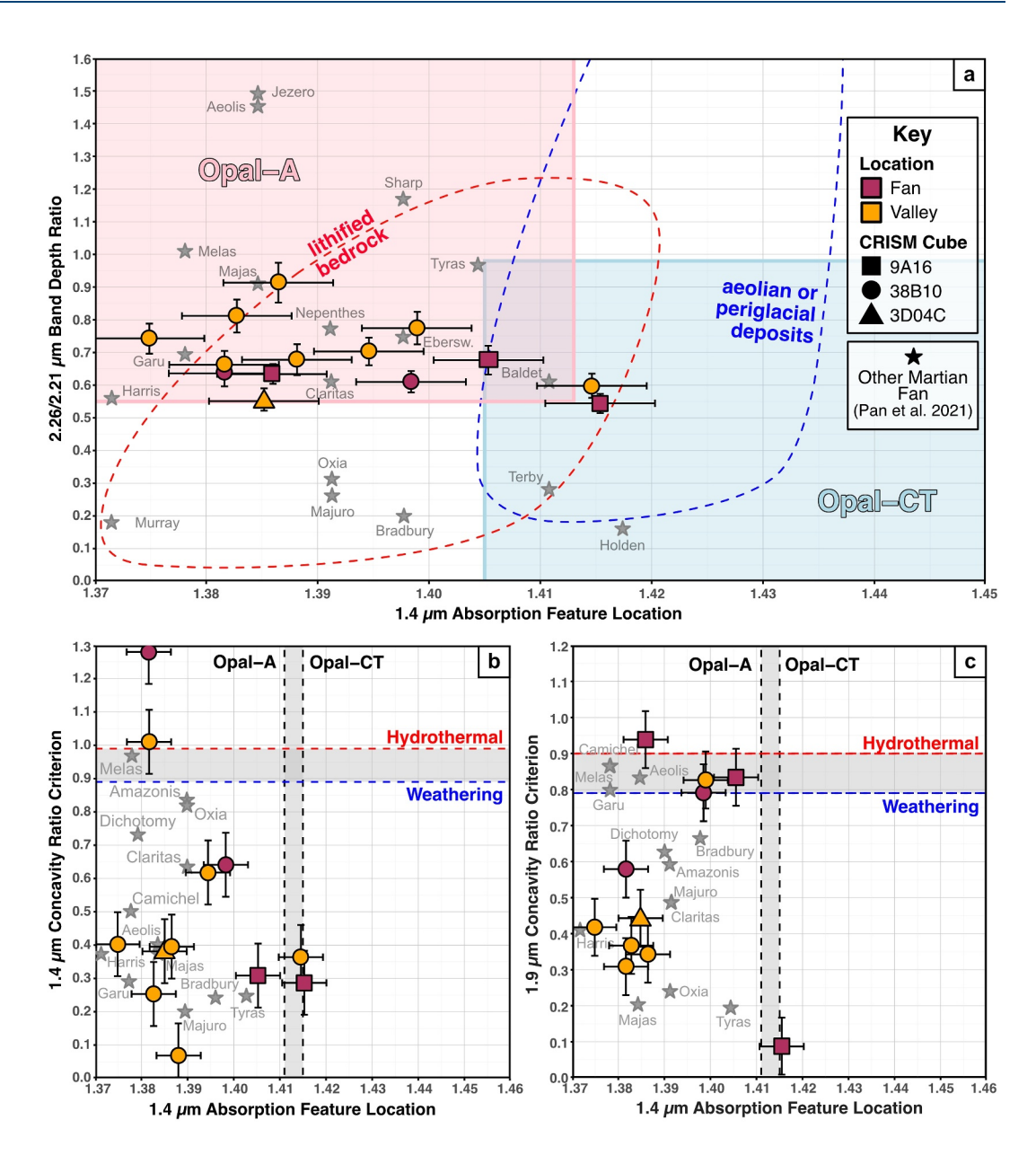


Figure 7. Crystallinity and origin of hydrated silica deposits in Oxia Planum from CRISM data. (a) Detection cluster in the opal-A (amorphous) field, indicating relatively immature silica. Data from Pan et al. (2021) and references therein (stars) show opal crystallinity and possible origin in other martian fan deposits. Boundaries of "lithified bedrock" and "aeolian or periglacial materials" CRISM detections from Sun and Milliken (2018) are also shown. Concavity ratio criterion values for the (b) 1.4 μm and (c) 1.9 μm absorption features as a measure of hydrothermal versus weathering origins for hydrated silica in Oxia Planum.

# 4.2. Opal-A Versus Opal-CT

The  $2.26/2.21~\mu m$  band depth ratio has been shown to be sensitive to changes in hydration induced by diurnal or seasonal atmospheric  $H_2O$  variations, and is thus broadly less reliable as a measure of crystallinity than the position of the  $1.4~\mu m$  absorption feature (Sun, 2017; Sun & Milliken, 2018). However, given that our results consistently plot within the opal-A field with both parameters (Figure 7), it is likely that they are reflective of a dominantly amorphous silica phase, and that any hydration-related variability is insufficient to obscure the broader spectral signature of low-crystallinity opaline materials.

MCNEIL ET AL. 12 of 20

Siliceous sinters in Icelandic hot springs have been shown to possess a range of CRC values, suggesting that low CRC values such as those associated with the HSU in Oxia Planum could be ascribed to either low-temperature hydrothermal activity or to continental weathering and are not genetically diagnostic (Pineau et al., 2023). However, given the lack of hydrothermal morphologies in the immediate area, the propensity of HSU to occur within areas typically associated with sedimentary deposition (topographic lows and the sedimentary fan), and the lack of unambiguous observations of hydrothermal minerals (e.g., mixtures of zeolites, prehnite, sulfates), we move forward with the interpretation that these are not hydrothermal in origin.

On Earth, maturation from opal-A to opal-CT is driven by higher pressures and temperatures found in deep oceanic environments, sedimentary basins, or in hydrothermal environments where circulating fluid allows for continual dissolution and reprecipitation of silica (e.g., Herdianita et al., 2000; Lynne & Campbell, 2004; Lynne et al., 2005; Rice et al., 1995; Williams et al., 1985) This process is thought to be similar on Mars, where subsequent aqueous alteration allows for gradual conversion of amorphous silica deposits through Ostwald Ripening to more crystalline varieties such as opal-CT, chalcedony, and microcrystalline quartz in <100-400 Ma (Rice et al., 2013; Sun & Milliken, 2018). Amorphous silica in Oxia Planum may therefore indicate that the aqueous processes associated with the HSU were the last major local geologic processes involving liquid water in the south of the landing site. It should be noted that opal maturation is highly variable on Earth; for example, opal-A deposits in Australia have been in contact with liquid water in warm climates for millions of years and have not undergone maturation into more crystalline varieties (Rey, 2013), and opal-CT deposits in Ethiopia formed diagenetically from the localized weathering of ignimbrites (Chauviré et al., 2019; Rondeau et al., 2012), showing that crystalline opal phases can form in situ through post-depositional processes without the need for a precursor opal-A deposit. Thus, in Oxia Planum, the presence of opal-A does not necessarily indicate immaturity or earlystage transformation; rather, it may reflect direct precipitation of amorphous silica under near-surface, lowtemperature conditions with minimal post-depositional alteration.

#### 4.3. Formation Hypotheses for Oxia Planum's Opal Deposits

Deposits of hydrated silica on Mars have been observed and associated with both delta and alluvial fan deposits (e.g., Pan et al., 2021), and in volcanic and hydrothermal environments, including impact-induced settings (Osinski et al., 2013; Skok et al., 2010; Squyres et al., 2008). Ancient sedimentary fans typically exhibit opalbearing deposits in localized regions that occur distally to the primary fan, laterally and/or stratigraphically (e.g., Camichel sedimentary fan; Pan et al., 2021), whereas relatively younger fans exhibit opaline silica detections corresponding to the entire deposit (e.g., Aeolis sedimentary fan; Pan et al., 2021). We did not directly detect opal within the bulk of the Oxia Planum sedimentary fan deposit using CRISM; however, discontinuous horizons of bright material within the fan (Figure 2e and Figure S2 in Supporting Information S1) suggest the presence of opal in discrete deposits above the main HSU. The limited exposure of these outcrops within and atop the fan means their composition cannot be confirmed using CRISM data; however, given their identical color and morphostratigraphic similarities to CRISM-confirmed opal detections (Figure S4 in Supporting Information S1), we proceed with the hypothesis that these are outcrops containing hydrated silica. As such, the Oxia Planum fan has a hydrated silica deposit at its base, typical of ancient sedimentary fans, and deposits (albeit localized and discrete) within its bulk, typical of younger stepped fans.

There are no major differences in opal crystallinity discernible from orbit between the sediment fan, or in the Pelso Chasma regions south of it (Figures 5–7). The sediment fan is a depositional feature, and Pelso Chasma is a topographic low, and both would have acted as local sedimentary sinks in the past, implying a strong palae-oenvironmental control on HSU formation. The similar stratigraphic and geographic locations of HSU across Oxia Planum could indicate contemporaneous emplacement, although the newly identified outcrops of HSU within the fan body occur at different stratigraphic horizons, showing that not all opal-bearing outcrops were initially formed at the same time. This added temporal complexity makes it difficult to constrain the formational mechanisms for outcrops of hydrated silica in Oxia Planum because the deposits could be the result of primary silica emplacement (e.g., through deposition of opal-rich sediments across multiple time intervals or through direct authigenic precipitation from surface waters), or secondary emplacement through post-emplacement modification of pre-existing sediments in the fan/topographic lows (e.g., through surface/shallow diagenetic processes and siliceous fluid circulation in a pedogenic or silcretization scenario).

MCNEIL ET AL. 13 of 20

21699100, 2025, 9, Downloaded from https://gupubs.onlinelibrary.wiley.com/doi/10.1029/20251908989 by Duch Zentrum F. Luft-U. Rawn Fahrt In D. Helmholtz Gemein., Wiley Online Library on [01/102025]. See the Terms and Conditions (https://onlinelibrary.wiley.com/term/

**Figure 8.** Schematic diagrams of authigenic precipitation scenarios in the Oxia Planum region. (a) Block diagram of the Oxia Planum sediment fan and Pelso Chasma (PC) region, showing flow from North and South Neocoogoon Vallis (NCV), respectively. Both the sediment fan and PC are the first opportunities for fast flowing water, carrying dissolved silica and detrital sediments (a<sup>1</sup>), to decrease in speed (a<sup>2</sup>) after entering Oxia Planum, resulting in increased silica precipitation in these regions. It is not known whether PC was open to the highlands through the valley that connects them in the present (location shown teal dotted arrow) at the time of hydrated silica-bearing unit emplacement. Water may also have entered PC through the inlets on its western margin, shown by light blue dotted arrows. (b) Schematic cross-section of the sediment fan, shown here as a delta, where the hydrated silica unit is prohibited from precipitation in the fast-flowing regions, except where local topography or other factors allow (dashed arrow), but can form in slower-flowing regions at the fan toe (dotted arrow). Post-depositional silica redistribution throughflow of groundwater through the fan is shown by white dotted arrows.

# 4.3.1. A Detrital Origin?

The HSU could represent detrital opal-rich sediments eroded from the highland catchment of the Oxia basin (Fawdon et al., 2022), transported by the Coogoon Valles system (Molina et al., 2017) before deposition as detrital material in topographically low regions and below the fan at the edge of the Noachian hinterland. A significant issue with this hypothesis is the absence of detections of hydrated silica-bearing source rocks in the Coogoon Valles catchment region (Turner et al., 2021), which is a common problem for opal-bearing sedimentary fans on Mars (Pan et al., 2021). Compared with other hydrated minerals such as phyllosilicates, hydrated silicarich rocks usually occur in small, thin, usually highly localized deposits, although the lack of CRISM detections of opal in the local catchment may be the result of dust occlusion, poor data coverage, or burial of the source rocks by later materials. Whilst hydrated silica itself has not been detected directly in the catchment, the catchment is heavily cratered and may contain deposits of silica-rich materials such as impact glass that can alter at low-to-moderate temperatures to form hydrated phases such as opal (e.g., Gin et al., 2021). The observation of possible HSU within the North Neocoogoon Vallis channel (Figure S2 in Supporting Information S1) could indicate detrital transport, but could equally be the result of authigenic precipitation of late-stage runoff waters in

MCNEIL ET AL. 14 of 20

topographic lows at the base of the channel, or post-fluvial silcretization (e.g., McCarthy & Ellery, 1995; Shaw & Nash, 1998) in the channel. These possibilities are discussed in the following subsections.

### 4.3.2. An Authigenic Origin?

The HSU could also have formed authigenically through in situ precipitation (Figure 8). The association of HSU deposits with the sedimentary fan and Pelso Chasma, and their apparent absence upstream or downstream, could suggest that the HSU marks the first significant slowdown of surface waters exiting the Coogoon Valles system (Figure 8a¹). This deceleration would have allowed dissolved silica to interact more effectively with the entrained sediment in the bedload, which acted as nucleation sites for silica precipitation (Figure 8a²). The slower water flow would also lead to higher local concentrations of dissolved silica, as it was not being transported away as rapidly. This localized deceleration could explain why the HSU is not continuous at the base of the fan: water would not have slowed down uniformly across the delta, leading to silica precipitation in specific topographic nooks or areas with varying water input or sediment load (Figure 8b). The observation of HSU in thin, discontinuous horizons within the fan suggests that, if they are authigenic in origin, precipitation occurred for short amounts of time in specific regions where conditions were favorable, such as at particular water depths where flow was diminished, where the water chemistry changed, or where sedimentary properties enhanced nucleation.

The presence of HSU below, within, and atop the fan in concentric deposits may result from precipitation at the water-rock interface in topographic lows or represent the final stages of the crater's water retention, where silica precipitation continued as water evaporated (e.g., McCarthy & Ellery, 1995; Shaw & Nash, 1998). In the former case, subsequent sediment deposition during fan progradation would have buried these silica deposits, creating discontinuous layers within the fan. Conversely, in Pelso Chasma, where there is no sedimentary fan, water likely decelerated more evenly, leading to more continuous silica deposits. In this model, both the sedimentary fan and Pelso Chasma areas acted as 'buffers' where the water slowed enough to facilitate silica precipitation. This model would also explain the lack of large deposits upstream, where water speeds may have been too fast for silica nucleation, and downstream, where much of the silica had already precipitated in the fan and Pelso Chasma regions. As a result, silica concentrations would have been much lower as the water exited these areas, especially if it entered another larger standing body of water in the Oxia Basin.

### 4.3.3. A Groundwater Silcretisation Origin?

The HSU may also be the result of post-depositional silcretization by groundwater in a subsurface environment. Here, significant volumes of silica-bearing solutions flowed through the sedimentary fan, permeating downwards, with opal precipitated as cement or as nodules in pore spaces (Figure 8b). In terrestrial fluviodeltaic environments, silcrete formation occurs when siliceous fluids recirculate through pre-existing sedimentary strata, often near the surface (Summerfield, 1983; Thiry & Milnes, 1991; Thiry & Ribet, 1999). Similar processes may have affected the Oxia Planum fan, resulting in post-depositional silica enrichment both in the thick basal HSU and in localized, higher stratigraphic outcrops. Stratigraphically controlled enrichment could explain the patchy distribution of hydrated silica across the fan. Higher-porosity features (e.g., lag deposits within palaeochannels, channel bars, or impact crater fill; Figures 2 and 4; Figure S3 in Supporting Information S1) may have served as conduits for silicarich fluids, enabling repeated saturation cycles and precipitation of hydrated silica as cement within finer-grained matrices. In coarser-grained settings, such as lags or gravelly fill, precipitation may have been concentrated within pore spaces, potentially forming opaline nodules. These mechanisms may have acted independently or in tandem, generating the complex vertical and lateral distribution of the opal-bearing horizons observed from orbit.

#### 4.3.4. A Pedogenic Silicification Origin?

Alternatively, silicification could have occurred through pedogenic processes at the near-surface, where weathering of silicate materials enriched the surface and near-surface in silica. Acidic weathering of Fe/Mg-rich phyllosilicates produces residues comprised primarily of amorphous silica of the same type we observe in Oxia Planum (Altheide et al., 2010), including other sulfate species that could contribute to the doublet feature observed in some spectra (Figure 6). Layered hydrated silica deposits have been observed associated with clay minerals in Morocco (Thiry et al., 2015), where the alteration of Mg-clays led to the leaching of Mg away from the upper alteration zone, enriching it in silica relative to adjacent strata. A similar process could have affected Oxia Planum, which would explain why the main HSU is exclusively observed stratigraphically above the clay-bearing

MCNEIL ET AL. 15 of 20

plains, but would not sufficiently explain the smaller discontinuous deposits within the sedimentary fan body itself. Additionally, widespread weathering would likely affect more than just the fan/valley regions, but no other weathering products of Fe/Mg-rich phyllosilicates are observed in Oxia Planum (e.g., Al-rich phyllosilicates dominate the upper ~10 m of bedrock in the Mawrth Vallis region (Noe Dobrea et al., 2010; Wray et al., 2008)), but are absent in Oxia Planum and would be expected if weathering progressed enough to produce hydrated silicabearing horizons. Although acidic weathering of phyllosilicates can generate opal-A deposits under low-pH conditions, similar products may also result from the alteration of basaltic material, and in situ identification of secondary mineral phases may be required to determine the precursor protolith (Altheide et al., 2010).

#### 4.4. Distal Hydrated Silica in Oxia Planum

Ultimately, the formation hypotheses for hydrated silica in Oxia Planum can only be tested in situ with a rover. Orbital data suggest that hydrated silica deposits at Oxia Planum are primarily amorphous (opal-A), which is similar to orbital observations of silica in Gale and Jezero Craters (e.g., Kepp et al., 2024; Tarnas et al., 2019). However, in situ observations from the Curiosity and Perseverance rovers, respectively, show that more crystalline phases (e.g., opal-CT, chalcedony, and pure quartz) are co-located with amorphous opal (Beck et al., 2025; Rapin et al., 2018). This raises the possibility that a more complex assemblage of silica phases may be present at Oxia Planum but remains undetectable from orbit. Future analyses by RFR will be critical in resolving this. The identified BCF outcrops may be ideal targets for geochemical investigation with the RFR *Pasteur* suite, and their proximity to the center of the landing ellipses means their investigation is a genuine possibility depending on the exact landing location.

If these deposits are related to the more extensive deposits of opal-A in Pelso Chasma and at the sedimentary fan, not only would they be extremely important astrobiological targets, but the nature of their outcrop-scale sedimentology could inform our understanding of basin-scale aqueous processes operating at the highland margin. For example, investigation of the relationships between sedimentary architectures and hydrated silica accumulations at the outcrop scale could indicate the depositional environment in which they were placed. Discrete layers of clastic opal entrained with other minerals would support detrital transport, and the degree of their sphericity and angularity could indicate their transport history. Opal coatings on sediment grains or clastic material embedded in an opal-rich matrix could indicate direct precipitation from solution. Additionally, opaline cement in pore spaces or as reprecipitated nodules that crosscut existing sedimentary architecture might indicate a post-depositional silcretization origin. Mixtures with clays could reveal insights into pedogenetic processes and/or complex interplays of detrital/authigenic origins at the local scale. Investigation of changes in opal crystallinity with stratigraphic depth at the outcrop scale (e.g., by interrogating the position of the 1.4 µm feature using Enfys), the RFR IR reflectance spectrometer (Grindrod et al., 2025; Vago et al., 2017), and MicrOmega-IR (Bibring et al., 2017) could elucidate the aqueous history of these deposits, and identify optimal drilling depths for the ExoMars Drill System to target in other astrobiologically relevant outcrops.

### 5. Conclusions

Oxia Planum—the future landing site of RFR—hosts deposits containing hydrated silica (opal) in two primary physiogeographical settings: (a) associated with the sedimentary fan, where opal is found at the lower contact between the fan and the underlying clay-bearing plains, and (b) in the topographic lows of Pelso Chasma, located south of the fan. Hyperspectral CRISM observations reveal that, regardless of location, the opal is predominantly amorphous (opal-A), and likely originated from weathering at the edge of the highlands. Investigating these opal-bearing outcrops with RFR's Pasteur suite could therefore offer a prime opportunity to detect biosignatures in relatively pristine deposits, making these deposits a key target in the mission's long-term strategy. Despite the presence of these astrobiologically promising features, however, the opal-bearing deposits confirmed by CRISM are located tens of kilometers from the 1-sigma 2028 landing ellipses and are therefore unrealistic strategic targets for RFR. To address this limitation, multispectral CaSSIS data have been used to identify additional rover-accessible outcrops within or near to the 3-sigma landing ellipses, with similar color, stratigraphic position, and texture. These outcrops may represent the rover's best—and possibly only—opportunity to sample opal-bearing materials in the region.

The spectral, morphological, and stratigraphic similarities between Oxia Planum's opal-bearing deposits suggest a shared emplacement mechanism. While detrital transport from the highlands cannot be entirely ruled out, the

MCNEIL ET AL. 16 of 20

most parsimonious explanation is authigenic precipitation, where silica precipitated as discrete particles or coatings on sediment as highland-derived water from Coogoon Valles slowed upon entering either Pelso Chasma or the fan area, or surface/near-surface silcretization processes involving silica-rich fluids enriching pre-existing sedimentary layers with hydrated silica in the form of cement or nodules. Determining which of these processes dominated here using RFR will be essential for reconstructing the aqueous and geological history of Oxia Planum.

# **Data Availability Statement**

All calibrated HiRISE (McEwen, 2007), CTX (Malin, 2007), and CRISM TRDR (Seelos, 2016a) and MTRDR data (Seelos, 2016b) used in this study were acquired from the Planetary Data System (PDS; https://pds.nasa.gov). All CaSSIS data (Thomas, 2021) were acquired from ESA's Planetary Science Archive (PSA; https://psa.esa.int/psa). A list of specific data products used is included in Table S1 in Supporting Information S1. Associated shapefile data are found in McNeil (2025).

# Acknowledgments References JDM is grateful to the UK Space Agency

for funding this study under Grant ST/

Y000471/1. PMG also acknowledges ST/

Y000471/1. LLT acknowledges funding

and support from the Canadian NSERC

Discovery Grant programme (RGPIN

2020-06418) and the Canadian Space

Agency (CSA) Planetary and Astronomy

Missions Co-Investigator (22EXPCOI3)

and FAST-Flights and Fieldwork for the

Advancement of Science and Technology

acknowledges UK Space Agency Funding

ST/V001965/1, ST/R001413/1, and ST/

W002736/1 and support by the European

acknowledges support from the Alexander

for their invaluable reviews, which greatly

additionally thank Lu Pan for generously

the University of Bern and funded through

hardware development was also supported

by the Italian Space Agency (ASI) (ASI-

INAF Agreement I/2020-17-HH.0), the

Padova, and the Space Research Center

(CBK) in Warsaw. Support from SGF

(Budapest), the University of Arizona

Grant ST/R003025/1 is also

acknowledged.

(Lunar and Planetary Lab.) and NASA are

also gratefully acknowledged. Operations support from the UK Space Agency under

INAF/Astronomical Observatory of

von Humboldt Foundation. The authors wish to thank Maxime Pineau and Lu Pan

(23FAUWESB78) programmes. PF

Space Agency through the ExoMars

Knowledge Science Program. VGR

helped improve the manuscript. We

sharing data on hydrated silica band

CaSSIS spacecraft and instrument engineering teams. CaSSIS is a project of

the Swiss Space Office via ESA's

PRODEX programme. The instrument

centers. The authors wish to thank the

Altheide, T. S., Chevrier, V. F., & Noe Dobrea, E. (2010). Mineralogical characterization of acid weathered phyllosilicates with implications for secondary martian deposits. *Geochimica et Cosmochimica Acta*, 74(21), 6232–6248. https://doi.org/10.1016/j.gca.2010.08.005

Armstrong, R. A. (1993). Remote sensing of submerged vegetation canopies for biomass estimation. *International Journal of Remote Sensing*, 14(3), 621–627. https://doi.org/10.1080/01431169308904363

Beck, P., Beyssac, O., Dehouck, E., Bernard, S., Pineau, M., Mandon, L., et al. (2025). From hydrated silica to quartz: Potential hydrothermal precipitates found in Jezero crater, Mars. Earth and Planetary Science Letters, 656, 119256. https://doi.org/10.1016/j.epsl.2025.119256

Bibring, J.-P., Hamm, V., Pilorget, C., Vago, J. L., & The MicrOmega Team. (2017). The MicrOmega investigation onboard ExoMars. Astro-biology, 17(6–7), 621–626. https://doi.org/10.1089/ast.2016.1642

Bibring, J. P., Langevin, Y., Mustard, J. F., Poulet, F., Arvidson, R., Gendrin, A., et al. (2006). Global mineralogical and aqueous Mars history derived from OMEGA/Mars express data. Science, 312(5772), 400–404. https://doi.org/10.1126/science.1122659

Bibring, J.-P., Soufflot, A., Berthé, M., Langevin, Y., Gondet, B., Drossart, P., et al. (2004). OMEGA: Observatoire pour la Minéralogie, l'Eau, les Glaces et l'Activité. In *Presented at the Mars Express: The scientific payload* (Vol. 1240, pp. 37–49).

Bickel, V. T., Thomas, N., Pommerol, A., Tornabene, L. L., El-Maarry, M. R., & Rangarajan, V. G. (2024). A global dataset of potential chloride deposits on Mars as identified by TGO CaSSIS. Scientific Data, 11(1), 845. https://doi.org/10.1038/s41597-024-03685-3

Bishop, J. L., Dobrea, E. Z. N., McKeown, N. K., Parente, M., Ehlmann, B. L., Michalski, J. R., et al. (2008). Phyllosilicate diversity and past aqueous activity revealed at Mawrth Vallis, Mars. Science, 321(5890), 830–833. https://doi.org/10.1126/science.1159699

Bishop, J. L., Gross, C., Danielsen, J., Parente, M., Murchie, S. L., Horgan, B., et al. (2020). Multiple mineral horizons in layered outcrops at Mawrth Vallis, Mars, signify changing geochemical environments on early Mars. *Icarus*, 341, 113634. https://doi.org/10.1016/j.icarus.2020.

Bohrmann, G., Abelmann, A., Gersonde, R., Hubberten, H., & Kuhn, G. (1994). Pure siliceous ooze, a diagenetic environment for early chert formation. *Geology*, 22(3), 207–210. https://doi.org/10.1130/0091-7613(1994)022<0207:PSOADE>2.3.CO;2

Boudreau, A. E., & Lynne, B. Y. (2012). The growth of siliceous sinter deposits around high-temperature eruptive hot springs. *Journal of Volcanology and Geothermal Research*, 247–248, 1–8. https://doi.org/10.1016/j.jvolgeores.2012.07.008

Brossier, J., Altieri, F., De Sanctis, M. C., Frigeri, A., Ferrari, M., De Angelis, S., et al. (2022). Constraining the spectral behavior of the clay-bearing outcrops in Oxia Planum, the landing site for ExoMars "Rosalind Franklin" rover. *Icarus*, 386, 115114. https://doi.org/10.1016/j.icarus.

Brown, L. D., Ray, A. S., & Thomas, P. S. (2003). <sup>29</sup>Si and <sup>27</sup>Al NMR study of amorphous and paracrystalline opals from Australia. *Journal of Non-Crystalline Solids*, 332(1–3), 242–248. https://doi.org/10.1016/j.jnoncrysol.2003.09.027

Burneau, A., Barres, O., Gallas, J. P., & Lavalley, J. C. (1990). Comparative study of the surface hydroxyl groups of fumed and precipitated silicas. 2. Characterization by infrared spectroscopy of the interactions with water. Langmuir, 6(8), 1364–1372. https://doi.org/10.1021/la00098a008 Butts, S. H. (2014). Silicification. In Reading and writing of the fossil record: Preservational pathways to exceptional fossilization (Vol. 20). The Paleontological Society. https://doi.org/10.1017/S1089332600002783

Carter, J., Riu, L., Poulet, F., Bibring, J.-P., Langevin, Y., & Gondet, B. (2023). A Mars orbital catalog of aqueous alteration signatures (MOCAAS). *Icarus*, 389, 115164. https://doi.org/10.1016/j.icarus.2022.115164

Chauviré, B., Houadria, M., Donini, A., Berger, B. T., Rondeau, B., Kritsky, G., & Lhuissier, P. (2020). Arthropod entombment in weathering-formed opal: New horizons for recording life in rocks. Scientific Reports, 10(1), 10575. https://doi.org/10.1038/s41598-020-67412-9

Chauviré, B., Rondeau, B., Alexandre, A., Chamard-Bois, S., La, C., & Mazzero, F. (2019). Pedogenic origin of precious opals from Wegel Tena (Ethiopia): Evidence from trace elements and oxygen isotopes. *Applied Geochemistry*, 101, 127–139. https://doi.org/10.1016/j.apgeochem. 2018.12.028

Chauviré, B., Rondeau, B., & Mangold, N. (2017). Near infrared signature of opal and chalcedony as a proxy for their structure and formation conditions. *European Journal of Mineralogy*, 29(3), 409–421. https://doi.org/10.1127/ejm/2017/0029-2614

Chavez, P. S. (1988). An improved dark-object subtraction technique for atmospheric scattering correction of multispectral data. *Remote Sensing of Environment*, 24(3), 459–479. https://doi.org/10.1016/0034-4257(88)90019-3

Christensen, P. R., Mehall, G. L., Silverman, S. H., Anwar, S., Cannon, G., Gorelick, N., et al. (2003). Miniature thermal emission spectrometer for the Mars exploration rovers. *Journal of Geophysical Research*, 108(E12), 8064. https://doi.org/10.1029/2003JE002117

Clark, R. N., King, T. V. V., Gorelick, N. S., & Geological, U. S. (1987). Automatic continuum analysis of reflectance spectra. In *Presented at the JPL Proceedings of the 3rd Airborne Imaging Spectrometer Data Analysis Workshop*.

Daubar, I. J., Dundas, C. M., Byrne, S., Geissler, P., Bart, G. D., McEwen, A. S., et al. (2016). Changes in blast zone albedo patterns around new martian impact craters. *Icarus*, 267, 86–105. https://doi.org/10.1016/j.icarus.2015.11.032

Davis, J. M., Balme, M. R., Fawdon, P., Grindrod, P. M., Favaro, E. A., Banham, S. G., & Thomas, N. (2023). Ancient alluvial plains at Oxia Planum, Mars. Earth and Planetary Science Letters, 601, 117904. https://doi.org/10.1016/j.epsl.2022.117904

MCNEIL ET AL. 17 of 20

- Duda, J.-P., Van Kranendonk, M. J., Thiel, V., Ionescu, D., Strauss, H., Schäfer, N., & Reitner, J. (2016). A rare glimpse of Paleoarchean life: Geobiology of an exceptionally preserved microbial mat facies from the 3.4 Ga Strelley Pool Formation, Western Australia. PLoS One, 11(1), e0147629. https://doi.org/10.1371/journal.pone.0147629
- Ehlmann, B. L., Mustard, J. F., Murchie, S. L., Bibring, J.-P., Meunier, A., Fraeman, A. A., & Langevin, Y. (2011). Subsurface water and clay mineral formation during the early history of Mars. *Nature*, 479(7371), 53–60. https://doi.org/10.1038/nature10582
- Ehlmann, B. L., Mustard, J. F., Swayze, G. A., Clark, R. N., Bishop, J. L., Poulet, F., et al. (2009). Identification of hydrated silicate minerals on Mars using MRO-CRISM: Geologic context near Nili Fossae and implications for aqueous alteration. *Journal of Geophysical Research*, 114(E2), E00D08. https://doi.org/10.1029/2009JE003339
- Eugster, H. P. (1969). Inorganic bedded cherts from the Magadi area, Kenya. Contributions to Mineralogy and Petrology, 22(1), 1–31. https://doi.org/10.1007/BF00388011
- Favaro, E. A., Balme, M. R., Davis, J. M., Grindrod, P. M., Fawdon, P., Barrett, A. M., & Lewis, S. R. (2021). The aeolian environment of the landing site for the ExoMars Rosalind Franklin Rover in Oxia Planum, Mars. *Journal of Geophysical Research: Planets*, 126(4), 2020JE006723. https://doi.org/10.1029/2020JE006723
- Fawdon, P., Balme, M., Davis, J., Bridges, J., Gupta, S., & Quantin-Nataf, C. (2022). Rivers and lakes in Western Arabia Terra: The fluvial catchment of the ExoMars 2022 rover landing site. *Journal of Geophysical Research: Planets*, 127(2), e2021JE007045. https://doi.org/10.1029/2021JE007045
- Fawdon, P., Grindrod, P., Orgel, C., Sefton-Nash, E., Adeli, S., Balme, M., et al. (2021). The geography of Oxia Planum. *Journal of Maps*, 17(2), 621–637. https://doi.org/10.1080/17445647.2021.1982035
- Garwood, R. J., Oliver, H., & Spencer, A. R. T. (2020). An introduction to the Rhynie chert. Geological Magazine, 157(1), 47–64. https://doi.org/10.1017/S0016756819000670
- Gin, S., Delaye, J.-M., Angeli, F., & Schuller, S. (2021). Aqueous alteration of silicate glass: State of knowledge and perspectives. npj Materials Degradation, 5(1), 1–20. https://doi.org/10.1038/s41529-021-00190-5
- Glotch, T. D., Bandfield, J. L., Christensen, P. R., Calvin, W. M., McLennan, S. M., Clark, B. C., et al. (2006). Mineralogy of the light-toned outcrop at Meridiani Planum as seen by the Miniature Thermal Emission Spectrometer and implications for its formation. *Journal of Geophysical Research*, 111(E12), E12S03. https://doi.org/10.1029/2005JE002672
- Gouzy, S., Phan, V. T. H., Bejach, L., Vinogradoff, V., Rondeau, B., Chauviré, B., et al. (2025). Preservation of biosignatures in opal probed by infrared nanospectroscopy. *Geochemical Perspectives Letters*, 35, 42–48. https://doi.org/10.7185/geochemlet.2522
- Grindrod, P. M., Cousins, C. R., & Gunn, M. (2025). Enfys: A near-infrared spectrometer for the ExoMars Rosalind Franklin Rover. In *Presented at the 56th Lunar and Planetary Science Conference, Houston, Texas* (Vol. 1840).
- Harris, E., Davis, J. M., Grindrod, P. M., Fawdon, P., & Roberts, A. L. (2024). A low albedo, thin, resistant unit in Oxia Planum, Mars: Evidence for an airfall deposit and late-stage groundwater activity at the ExoMars rover landing site. *Journal of Geophysical Research: Planets*, 129(11), e2024JE008527. https://doi.org/10.1029/2024JE008527
- Herdianita, N. R., Browne, P. R. L., Rodgers, K. A., & Campbell, K. A. (2000). Mineralogical and textural changes accompanying ageing of silica sinter. *Mineralium Deposita*, 35(1), 48–62. https://doi.org/10.1007/s001260050005
- Kepp, M., Pan, L., Frydenvang, J., & Bizzarro, M. (2024). Orbital identification of widespread hydrated silica deposits in Gale crater. Earth and Planetary Science Letters, 648, 119082. https://doi.org/10.1016/j.epsl.2024.119082
- Kokaly, R. F., Clark, R. N., Swayze, G. A., Livo, K. E., Hoefen, T. M., Pearson, N. C., et al. (2017). USGS Spectral Library Version 7 (Report No. 1035) (p. 68). https://doi.org/10.3133/ds1035
- Langer, K., & Flörke, O. W. (1974). Near infrared absorption spectra (4000–9000 cm<sup>-1</sup>) of opals and the role of "water" in these SiO<sub>2</sub>-nH<sub>2</sub>O minerals. Fortschritte der Mineralogie, 52(1), 17–51.
- Lynne, B. Y., & Campbell, K. A. (2004). Morphologic and mineralogic transitions from opal-A to opal-CT in low-temperature siliceous sinter diagenesis, Taupo Volcanic Zone, New Zealand. *Journal of Sedimentary Research*, 74(4), 561–579. https://doi.org/10.1306/011704740561
- Lynne, B. Y., Campbell, K. A., Moore, J. N., & Browne, P. R. L. (2005). Diagenesis of 1900-year-old siliceous sinter (opal-A to quartz) at Opal Mound, Roosevelt Hot Springs, Utah, U.S.A. Sedimentary Geology, 179(3), 249–278. https://doi.org/10.1016/j.sedgeo.2005.05.012
- Malin, M. C. (2007). MRO Context Camera Experiment Data Record Level 0 V1.0 (Version V1.0) [Dataset]. NASA Planetary Data System. https://doi.org/10.17189/1520266
- Malin, M. C., Bell, J. F., Cantor, B. A., Caplinger, M. A., Calvin, W. M., Clancy, R. T., et al. (2007). Context Camera Investigation on board the Mars Reconnaissance Orbiter. *Journal of Geophysical Research*, 112(5), 1–25. https://doi.org/10.1029/2006JE002808
- Mandon, L., Parkes Bowen, A., Quantin-Nataf, C., Bridges, J. C., Carter, J., Pan, L., et al. (2021). Morphological and spectral diversity of the clay-bearing unit at the ExoMars landing site Oxia Planum. Astrobiology, 21(4), 464–480. https://doi.org/10.1089/ast.2020.2292
- Marzo, G. A., Davila, A. F., Tornabene, L. L., Dohm, J. M., Fairén, A. G., Gross, C., et al. (2010). Evidence for Hesperian impact-induced hydrothermalism on Mars. *Icarus*, 208(2), 667–683. https://doi.org/10.1016/j.icarus.2010.03.013
- McCarthy, T. S., & Ellery, W. N. (1995). Sedimentation on the distal reaches of the Okavango Fan, Botswana, and its bearing on calcrete and silcrete (ganister) formation. *Journal of Sedimentary Research*, 65(1a), 77–90. https://doi.org/10.1306/D426802C-2B26-11D7-8648000102C1865D
- McEwen, A. S. (2007). MRO Mars high resolution image science experiment EDR V1.0 (Version V1.0) [Dataset]. NASA Planetary Data System. https://doi.org/10.17189/1520179
- McEwen, A. S., Eliason, E. M., Bergstrom, J. W., Bridges, N. T., Hansen, C. J., Delamere, W. A., et al. (2007). Mars reconnaissance orbiter's high resolution imaging science experiment (HiRISE). *Journal of Geophysical Research*, 112(5), 1–40. https://doi.org/10.1029/2005JE002605
- McGuire, P. C., Bishop, J. L., Brown, A. J., Fraeman, A. A., Marzo, G. A., Morgan, M. F., et al. (2009). An improvement to the volcano-scan algorithm for atmospheric correction of CRISM and OMEGA spectral data. *Planetary and Space Science*, 57(7), 809–815. https://doi.org/10.1016/j.pss.2009.03.007
- McMahon, S., van Smeerdijk Hood, A., & McIlroy, D. (2017). The origin and occurrence of subaqueous sedimentary cracks. *Geological Society Special Publication*, 448(1), 285–309. https://doi.org/10.1144/SP448.15
- McNeil, J. D., (2025). CRISM measurement data for "Hydrated Silica in Oxia Planum, Mars" [Dataset]. Figshare. https://doi.org/10.6084/m9. figshare.29371346
- McNeil, J. D., Fawdon, P., Balme, M. R., Coe, A. L., & Thomas, N. (2022). Mounds in Oxia Planum: The burial and exhumation of the ExoMars rover landing site. *Journal of Geophysical Research: Planets*, 127(11), e2022JE007246. https://doi.org/10.1029/2022JE007246
- Milliken, R. E., Grotzinger, J. P., & Thomson, B. J. (2010). Paleoclimate of Mars as captured by the stratigraphic record in Gale Crater. Geophysical Research Letters, 37(4), L04201. https://doi.org/10.1029/2009GL041870
- Milliken, R. E., Swayze, G. A., Arvidson, R. E., Bishop, J. L., Clark, R. N., Ehlmann, B. L., et al. (2008). Opaline silica in young deposits on Mars. *Geology*, 36(11), 847–850. https://doi.org/10.1130/G24967A.1

MCNEIL ET AL. 18 of 20

21699100, 2025, 9, Downloa

- Molina, A., López, I., Prieto-Ballesteros, O., Fernández-Remolar, D., de Pablo, M. Á., & Gómez, F. (2017). Coogoon Valles, western Arabia Terra: Hydrological evolution of a complex Martian channel system. *Icarus*, 293, 27–44. https://doi.org/10.1016/j.icarus.2017.04.002
- Morgan, M. F., Seelos, F. P., & Murchie, S. L. (2017). The CRISM analysis toolkit (CAT): Overview and recent updates. In *Presented at the 3rd Planetary Data Workshop 2017*. Northern Arizona University.
- Murchie, S., Arvidson, R., Bedini, P., Beisser, K., Bibring, J. P., Bishop, J., et al. (2007). Compact Connaissance Imaging Spectrometer for Mars (CRISM) on Mars Reconnaissance Orbiter (MRO). *Journal of Geophysical Research*, 112(5), 1–57. https://doi.org/10.1029/2006JE002682
- Mustard, J. F., Murchie, S. L., Pelkey, S. M., Ehlmann, B. L., Milliken, R. E., Grant, J. A., et al. (2008). Hydrated silicate minerals on Mars observed by the Mars Reconnaissance Orbiter CRISM instrument. *Nature*, 454(7202), 305–309. https://doi.org/10.1038/nature07097
- Noe Dobrea, E. Z., Bishop, J. L., McKeown, N. K., Fu, R., Rossi, C. M., Michalski, J. R., et al. (2010). Mineralogy and stratigraphy of phyllosilicate-bearing and dark mantling units in the greater Mawrth Vallis/west Arabia Terra area: Constraints on geological origin. *Journal of Geophysical Research*, 115(E7), E00D19. https://doi.org/10.1029/2009je003351
- Oehler, J. H. (1979). Chapter 7.3 Deposition and diagenesis of biogenic silica. In P. A. Trudinger & D. J. Swaine (Eds.), Studies in environmental science (Vol. 3, pp. 467–483). Elsevier. https://doi.org/10.1016/S0166-1116(08)71068-9
- Orange, F., Lalonde, S. V., & Konhauser, K. O. (2013). Experimental simulation of evaporation-driven silica sinter formation and microbial silicification in hot spring systems. *Astrobiology*, 13(2), 163–176. https://doi.org/10.1089/ast.2012.0887
- Orange, F., Westall, F., Disnar, J.-R., Prieur, D., Bienvenu, N., Le Romancer, M., & Défarge, C. (2009). Experimental silicification of the extremophilic Archaea *Pyrococcus abyssi* and *Methanocaldococcus jannaschii*: Applications in the search for evidence of life in early Earth and extraterrestrial rocks. *Geobiology*, 7(4), 403–418. https://doi.org/10.1111/j.1472-4669.2009.00212.x
- Osinski, G. R., Tornabene, L. L., Banerjee, N. R., Cockell, C. S., Flemming, R., Izawa, M. R. M., et al. (2013). Impact-generated hydrothermal systems on Earth and Mars. *Icarus*, 224(2), 347–363. https://doi.org/10.1016/j.icarus.2012.08.030
- Pan, L., Carter, J., Quantin-Nataf, C., Pineau, M., Chauviré, B., Mangold, N., et al. (2021). Voluminous silica precipitated from martian waters during late-stage aqueous alteration. The Planetary Science Journal, 2(2), 65. https://doi.org/10.3847/PSJ/abe541
- Parkes-Bowen, A., Bridges, J., Tornabene, L., Mandon, L., Quantin-Nataf, C., Patel, M. R., et al. (2022). A CaSSIS and HiRISE map of the Claybearing Unit at the ExoMars 2022 landing site in Oxia Planum. *Planetary and Space Science*, 214, 105429. https://doi.org/10.1016/j.pss.2022. 105429
- Pineau, M., Chauviré, B., & Rondeau, B. (2023). Near-infrared signature of hydrothermal opal: A case study of Icelandic silica sinters. *European Journal of Mineralogy*, 35(6), 949–967. https://doi.org/10.5194/ejm-35-949-2023
- Pineau, M., Le Deit, L., Chauviré, B., Carter, J., Rondeau, B., & Mangold, N. (2020). Toward the geological significance of hydrated silica detected by near infrared spectroscopy on Mars based on terrestrial reference samples. *Icarus*, 347, 113706. https://doi.org/10.1016/j.icarus. 2020.113706
- Poulet, F., Bibring, J. P., Mustard, J. F., Gendrin, A., Mangold, N., Langevin, Y., et al. (2005). Phyllosilicates on Mars and implications for early martian climate. *Nature*, 438(7068), 623–627. https://doi.org/10.1038/nature04274
- Quantin-Nataf, C., Carter, J., Mandon, L., Thollot, P., Balme, M., Volat, M., et al. (2021). Oxia Planum: The landing site for the ExoMars "Rosalind Franklin" rover mission: Geological context and prelanding interpretation. *Astrobiology*, 21(3), 345–366. https://doi.org/10.1089/ast.2019.2191
- Rangarajan, V. G., Tornabene, L. L., Osinski, G. R., Conway, S. J., Seelos, F. P., Silvestro, S., et al. (2023). Change detection and monitoring of active Martian surface phenomena with the Colour and Stereo Surface Imaging System (CaSSIS) onboard the ExoMars Trace Gas Orbiter (TGO). *Icarus*. 394. 115443. https://doi.org/10.1016/j.icarus.2023.115443
- Rangarajan, V. G., Tornabene, L. L., Osinski, G. R., Dundas, C. M., Beyer, R. A., Herkenhoff, K. E., et al. (2024). Novel quantitative methods to enable multispectral identification of high-purity water ice exposures on Mars using High Resolution Imaging Science Experiment (HiRISE) images. *Icarus*, 419, 115849. https://doi.org/10.1016/j.icarus.2023.115849
- Rapin, W., Chauviré, B., Gabriel, T. S. J., McAdam, A. C., Ehlmann, B. L., Hardgrove, C., et al. (2018). In situ analysis of opal in Gale Crater, Mars. Journal of Geophysical Research: Planets. 123(8), 1955–1972. https://doi.org/10.1029/2017JE005483
- Rey, P. F. (2013). Opalisation of the Great Artesian Basin (central Australia): An Australian story with a Martian twist. Australian Journal of Earth Sciences, 60(3), 291–314. https://doi.org/10.1080/08120099.2013.784219
- Rice, M. S., Cloutis, E. A., Bell, J. F., Bish, D. L., Horgan, B. H., Mertzman, S. A., et al. (2013). Reflectance spectra diversity of silica-rich materials: Sensitivity to environment and implications for detections on Mars. *Icarus*, 223(1), 499–533. https://doi.org/10.1016/j.icarus. 2012.09.021
- Rice, S. B., Freund, H., Huang, W. L., Clouse, J. A., & Isaacs, C. M. (1995). Application of Fourier transform infrared spectroscopy to silica diagenesis; the opal-A to opal-CT transformation. *Journal of Sedimentary Research*, 65(4a), 639–647. https://doi.org/10.1306/D4268185-2B26-11D7-8648000102C1865D
- Roberts, A., Gupta, S., Fawdon, P., Banham, S., Davis, J., & Harris, E. (2024). Reconstructing depositional environments of the sediment fan in Oxia Planum, Mars (No. EPSC2024-1171). In *Presented at the EPSC2024, copernicus meetings*. https://doi.org/10.5194/epsc2024-1171
- Roberts, A. L., Fawdon, P., & Mirino, M. (2021). Impact crater degradation, Oxia Planum, Mars. *Journal of Maps*, 17(2), 569–578. https://doi.org/10.1080/17445647.2021.1976685
- Rondeau, B., Cenki-Tok, B., Fritsch, E., Mazzero, F., Gauthier, J.-P., Bodeur, Y., et al. (2012). Geochemical and petrological characterization of gem opals from Wegel Tena, Wollo, Ethiopia: Opal formation in an Oligocene soil. *Geochemistry: Exploration, Environment, Analysis*, 12(2), 93–104. https://doi.org/10.1144/1467-7873/10-MINDEP-058
- Ruff, S. W., Farmer, J. D., Calvin, W. M., Herkenhoff, K. E., Johnson, J. R., Morris, R. V., et al. (2011). Characteristics, distribution, origin, and significance of opaline silica observed by the Spirit rover in Gusev crater, Mars. *Journal of Geophysical Research*, 116(E7), E00F23. https://doi.org/10.1029/2010JE003767
- Savitzky, A., & Golay, M. J. E. (1964). Smoothing and differentiation of data by simplified least squares procedures. *Analytical Chemistry*, 36(8), 1627–1639. https://doi.org/10.1021/ac60214a047
- Schopf, J. W. (1993). Microfossils of the Early Archean Apex chert: New evidence of the antiquity of life. Science, 260(5108), 640–646. https://doi.org/10.1126/science.260.5108.640
- Seelos, F. P. (2016a). MRO CRISM map-projected targeted reduced data record V1.0 (Version V1.0) [Dataset]. NASA Planetary Data System. https://doi.org/10.17189/1519470
- Seelos, F. P. (2016b). MRO CRISM targeted reduced data record V1.0 (Version V1.0) [Dataset]. NASA Planetary Data System. https://doi.org/10. 17189/1519450
- Seelos, F. P., Seelos, K. D., Murchie, S. L., Novak, M. A. M., Hash, C. D., Morgan, M. F., et al. (2024). The CRISM investigation in Mars orbit: Overview, history, and delivered data products. *Icarus*, 419, 115612. https://doi.org/10.1016/j.icarus.2023.115612

MCNEIL ET AL. 19 of 20

- Seelos, K. D., Arvidson, R. E., Jolliff, B. L., Chemtob, S. M., Morris, R. V., Ming, D. W., & Swayze, G. A. (2010). Silica in a Mars analog environment: Ka'u Desert, Kilauea Volcano, Hawaii. *Journal of Geophysical Research*, 115(E4), E00D15. https://doi.org/10.1029/2009IF003347
- Shaw, P. A., & Nash, D. J. (1998). Dual mechanisms for the formation of fluvial silcretes in the distal reaches of the Okavango Delta fan, Botswana. Earth Surface Processes and Landforms, 23(8), 705–714. https://doi.org/10.1002/(SICI)1096-9837(199808)23:8<705::AID-ESP875>3.0.CO:2-7
- Skok, J. R., Mustard, J. F., Ehlmann, B. L., Milliken, R. E., & Murchie, S. L. (2010). Silica deposits in the Nili Patera caldera on the Syrtis Major volcanic complex on Mars. *Nature Geoscience*, 3(12), 838–841. https://doi.org/10.1038/ngeo990
- Squyres, S. W., Arvidson, R. E., Ruff, S., Gellert, R., Morris, R. V., Ming, D. W., et al. (2008). Detection of silica-rich deposits on Mars. *Science*, 320(5879), 1063–1067. https://doi.org/10.1126/science.1155429
- Steinier, J., Termonia, Y., & Deltour, J. (1972). Smoothing and differentiation of data by simplified least square procedure. *Analytical Chemistry*, 44(11), 1906–1909. https://doi.org/10.1021/ac60319a045
- Sucharski, T., Mapel, J., jcwbacker, Kristin, Lee, K., AgoinsUSGS, et al. (2020). USGS-Astrogeology/ISIS3: ISIS 4.2.0 Public Release (Version 4.2.0) [Dataset]. Zenodo. https://doi.org/10.5281/zenodo.3962369
- Summerfield, M. A. (1983). Silcrete as a palaeoclimatic indicator: Evidence from southern Africa. *Palaeogeography, Palaeoclimatology, Palaeoecology, 41*(1–2), 65–79. https://doi.org/10.1016/0031-0182(83)90076-7
- Sun, V. (2017). Clays and opals on Mars: Implications for water-rock interactions through time. Brown University. https://doi.org/10.7301/
- Sun, V. Z., & Milliken, R. E. (2018). Distinct geologic settings of opal-A and more crystalline hydrated silica on Mars. *Geophysical Research Letters*, 45(19), 10221–10228. https://doi.org/10.1029/2018GL078494
- Sun, V. Z., & Milliken, R. E. (2020). Characterizing the mineral assemblages of hot spring environments and applications to Mars orbital data. Astrobiology, 20(4), 453–474. https://doi.org/10.1089/ast.2018.2003
- Tao, Y., Muller, J.-P., Conway, S. J., & Xiong, S. (2021). Large area high-resolution 3D mapping of Oxia Planum: The landing site for the
- ExoMars Rosalind Franklin rover. Remote Sensing, 13(16), 3270. https://doi.org/10.3390/rs13163270
  Tarnas, J. D., Mustard, J. F., Lin, H., Goudge, T. A., Amador, E. S., Bramble, M. S., et al. (2019). Orbital identification of hydrated silica in Jezero
- crater, Mars. Geophysical Research Letters, 46(22), 12771–12782. https://doi.org/10.1029/2019GL085584

  Thiry, M., Milnes, A., & Ben Brahim, M. (2015). Pleistocene cold climate groundwater silicification, Jbel Ghassoul region, Missour Basin, Morocco. Journal of the Geological Society, 172(1), 125–137. https://doi.org/10.1144/jgs2014-033
- Thiry, M., & Milnes, A. R. (1991). Pedogenic and groundwater silcretes at Stuart Creek Opal Field, South Australia. *Journal of Sedimentary Research*, 61(1), 111–127. https://doi.org/10.1306/d426769f-2b26-11d7-8648000102c1865d
- Thiry, M., & Ribet, I. (1999). Groundwater silicification in Paris Basin limestones: Fabrics, mechanisms, and modeling. *Journal of Sedimentary*
- Research, 69(1), 171–183. https://doi.org/10.1306/d42689a5-2b26-11d7-8648000102c1865d
  Thomas, N. (2021). ExoMars 2016 CaSSIS calibrated Data Product Collection (Version 2.2) [Dataset]. European Space Agency. https://doi.org/
- 10.5270/esa-da0ic0t
  Thomas N. Cramonaca G. Ziatha P. Garbar M. Brindli M. Bruno G. et al. (2017). The colour and starso surface imaging system (CaSSIS)
- Thomas, N., Cremonese, G., Ziethe, R., Gerber, M., Brändli, M., Bruno, G., et al. (2017). The colour and stereo surface imaging system (CaSSIS) for the ExoMars trace gas orbiter. Space Science Reviews, 212(3–4), 1897–1944. https://doi.org/10.1007/s11214-017-0421-1
- Tornabene, L. L., Conway, S., Cremonese, G., Lucchetti, A., Munaretto, G., McEwen, A., et al. (2021). Potential detection of exposed Martian water ice with multispectral images from the Exomars colour and stereo surface imaging system. In *Presented at the 52nd Lunar and Planetary Science Conference 2021*.
- Tornabene, L. L., Rangarajan, V. G., Seelos, F. P., Douté, S., Munaretto, G., Viviano, C., et al. (2022). Application of an empirical dark [shadow] subtraction method to CRISM VNRI+IR data as a supplemental method for spectral analysis of the surface. In *Presented at the 53rd Lunar and Planetary Science Conference* 2022 (Vol. 2330).
- Tornabene, L. L., Seelos, F. P., Pommerol, A., Thomas, N., Caudill, C. M., Becerra, P., et al. (2018). Image simulation and assessment of the colour and spatial capabilities of the Colour and Stereo Surface Imaging System (CaSSIS) on the ExoMars Trace Gas Orbiter. *Space Science Reviews*, 214(1), 18. https://doi.org/10.1007/s11214-017-0436-7
- Turner, S. M. R., Fawdon, P., & Davis, J. M. (2021). Mineralogy of the Oxia Planum catchment area on Mars and its relevance to the ExoMars Rosalind Franklin rover mission (Vol. Abstract 2490). In *Presented at the 52nd Lunar and Planetary Science Conference 2021*.
- Vago, J. L., Westall, F., Coates, A. J., Jaumann, R., Korablev, O., Ciarletti, V., et al. (2017). Habitability on early Mars and the search for biosignatures with the ExoMars rover. Astrobiology, 17(6–7), 471–510. https://doi.org/10.1089/ast.2016.1533
- Viviano-Beck, C. E., Seelos, F. P., Murchie, S. L., Kahn, E. G., Seelos, K. D., Taylor, H. W., et al. (2014). Revised CRISM spectral parameters and summary products based on the currently detected mineral diversity on Mars. *Journal of Geophysical Research: Planets*, 119(6), 1403–1431. https://doi.org/10.1002/2014JE004627
- Voigt, J. R. C., Sun, V. Z., Viviano, C. E., & Stack, K. M. (2024). Investigating Hydrated silica in Syrtis Major, Mars: Implications for the longevity of water-rock interaction. Geophysical Research Letters, 51(18), e2024GL108610. https://doi.org/10.1029/2024GL108610
- Wicaksono, P., & Hafizt, M. (2018). Dark target effectiveness for dark-object subtraction atmospheric correction method on mangrove above-ground carbon stock mapping. *IET Image Processing*, 12(4), 582–587. https://doi.org/10.1049/iet-ipr.2017.0295
- Williams, L. A., Parks, G. A., & Crerar, D. A. (1985). Silica diagenesis; I, Solubility controls. *Journal of Sedimentary Research*, 55(3), 301–311. https://doi.org/10.1306/212F86AC-2B24-11D7-8648000102C1865D
- Wray, J. J., Ehlmann, B. L., Squyres, S. W., Mustard, J. F., & Kirk, R. L. (2008). Compositional stratigraphy of clay-bearing layered deposits at Mawrth Vallis, Mars. Geophysical Research Letters, 35(12), 2–7. https://doi.org/10.1029/2008GL034385

MCNEIL ET AL. 20 of 20